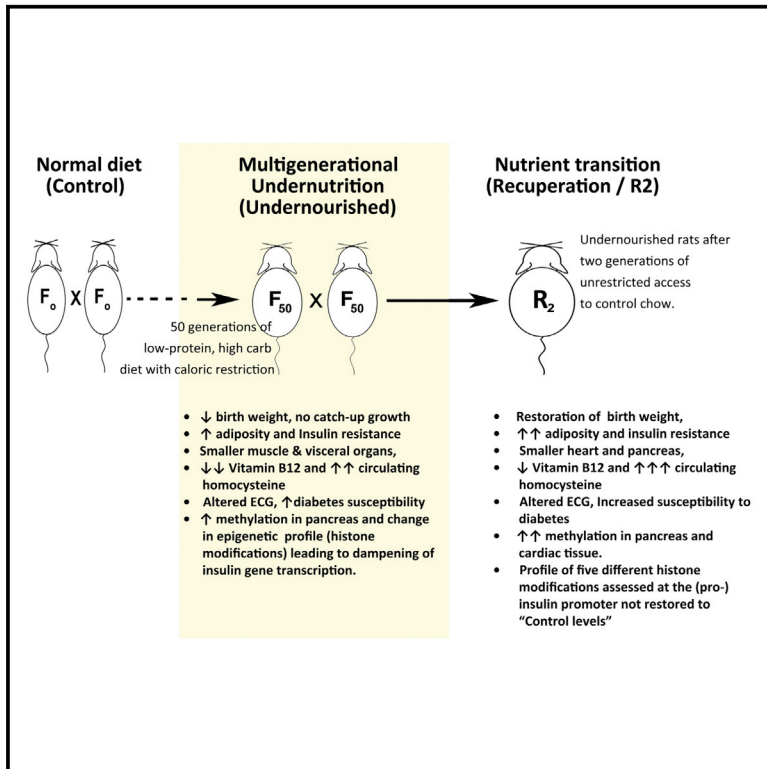On the cover:

Long-term consequences of undernutrition on metabolism.

On pp. 312–319 of this issue, Hardikar et al. use a rat model of undernutrition over 50 generations (a 12-year-long experiment), which closely mimics human populations in developing countries, to study how environmental impacts can be transmitted across generations. Undernourished rats are more susceptible to obesity and diabetes, and these metabolic abnormalities, associated with epigenetic changes, are not reversed following unrestricted access to normal chow in two subsequent generations. The cover image depicts the concept of intergenerational inheritance and its association with histone modifications at key metabolic genes.

Cell Metabolism

Multigenerational Undernutrition Increases Susceptibility to Obesity and Diabetes that Is Not Reversed after Dietary Recuperation

Graphical Abstract

Highlights

- Undernourished rats are protein / calorie-restricted for 50 generations

- Recuperation rats are generated by feeding normal chow for two more generations

- Undernourished and Recuperation rats show multiple markers of metabolic disease

- Metabolic / epigenetic alterations are not reversed following nutrient recuperation

Authors

Anandwardhan A. Hardikar,
Sarang N. Satoor,
Mahesh S. Karandikar, ...,
Anthony C. Keech, Alicia J. Jenkins,
Chittaranjan S. Yajnik

Correspondence

anand.hardikar@ctc.usyd.edu.au

In Brief

In a rat model of undernutrition over 50 generations, closely mimicking human populations in developing countries, Hardikar et al. show that undernourished rats display metabolic abnormalities associated with epigenetic changes, which are not reversed following unrestricted access to normal chow in two subsequent generations.

CellPress

Short Article

CellPress

Multigenerational Undernutrition Increases Susceptibility to Obesity and Diabetes that Is Not Reversed after Dietary Recuperation

Anandwardhan A. Hardikar,[1,11,*] Sarang N. Satoor,[1,2,11] Mahesh S. Karandikar,[3,4,11] Mugdha V. Joglekar,[1,11]
Amrutesh S. Puranik,[2,12] Wilson Wong,[1] Sandeep Kumar,[2] Amita Limaye,[2,5] Dattatray S. Bhat,[6] Andrzej S. Januszewski,[1]
Malati R. Umrani,[2] Amaresh K. Ranjan,[7] Kishori Apte,[8] Pranav Yajnik,[9] Ramesh R. Bhonde,[2,10] Sanjeev Galande,[5]
Anthony C. Keech,[1] Alicia J. Jenkins,[1] and Chittaranjan S. Yajnik[6]
[1]NHMRC Clinical Trials Centre, University of Sydney, Sydney, NSW 2050, Australia
[2]National Center for Cell Science, Ganeshkhind Road, Pune 411007, India
[3]Department of Physiology, DY Patil Medical College, DPU, Pimpri, Pune 411018, India
[4]Department of Physiology, BJ Medical College, Pune 411011, India
[5]Indian Institute of Science Education and Research (IISER), Dr Homi Bhabha Road, Pashan, Pune 411008, India
[6]Diabetes Unit, KEM Hospital, Rasta Peth, Pune 411011, India
[7]Cardiovascular Institute, Mount Sinai School of Medicine, New York, NY 10029, USA
[8]National Toxicology Center, 36/1/1 MN199, Vadgaon Khurd, Singhgad Road, Pune 411041, India
[9]Department of Biostatistics, University of Michigan, Ann Arbor, Michigan 48109, USA
[10]Manipal Institute of Regenerative Medicine, Manipal University, Bangalore, India
[11]Co-first author
[12]Present address: Robert & Arlene Kogod Center on Aging, Mayo Clinic, Rochester, MN 55905, USA
*Correspondence: anand.hardikar@ctc.usyd.edu.au
http://dx.doi.org/10.1016/j.cmet.2015.06.008

SUMMARY

People in developing countries have faced multigenerational undernutrition and are currently undergoing major lifestyle changes, contributing to an epidemic of metabolic diseases, though the underlying mechanisms remain unclear. Using a Wistar rat model of undernutrition over 50 generations, we show that Undernourished rats exhibit low birth-weight, high visceral adiposity (DXA/MRI), and insulin resistance (hyperinsulinemic-euglycemic clamps), compared to age-/gender-matched control rats. Undernourished rats also have higher circulating insulin, homocysteine, endotoxin and leptin levels, lower adiponectin, vitamin B12 and folate levels, and an 8-fold increased susceptibility to Streptozotocin-induced diabetes compared to control rats. Importantly, these metabolic abnormalities are not reversed after two generations of unrestricted access to commercial chow (nutrient recuperation). Altered epigenetic signatures in insulin-2 gene promoter region of Undernourished rats are not reversed by nutrient recuperation, and may contribute to the persistent detrimental metabolic profiles in similar multigenerational undernourished human populations.

INTRODUCTION

The burden of type 2 diabetes mellitus (T2D) is increasing worldwide, particularly in developing countries, where >70% of the global burden of T2D is predicted to exist by 2030 (Echouffo-Tcheugui and Dagogo-Jack, 2012). Although reasons for the increasing rates of T2D in developing countries are not fully elucidated, important factors include lifestyle changes involving rural-to-urban migration ("urbanization"), intra-uterine undernutrition, and fetal programming.

During the past two decades, increasing evidence arising from multiple clinical studies conducted by the research teams of Yajnik and Barker support an important role of early life undernutrition, and specifically disturbances of one-carbon metabolism, in the heightened susceptibility of (Asian) Indians to T2D at a younger age, and in the absence of generalized obesity (Yajnik et al., 1995, 2003, 2014; Yajnik and Deshmukh, 2012). These studies have highlighted body composition and nutritional-metabolic peculiarities of multigenerationally undernourished Indians: a thin-fat (low lean mass, high fat mass) phenotype compared to Europeans, with predominant visceral deposition of fat. This body composition is strongly associated with insulin resistance and related metabolic-endocrine abnormalities. Importantly, this "thin-fat" phenotype was present at birth and, therefore, programmed during intrauterine life, possibly through epigenetic mechanisms over multiple generations. Maternal intergenerational undernutrition, evident in stunting, low BMI, and a disturbance of dietary methyl donors (low protein and vitamin B_{12} and high folate status, related to vegetarian diets) appear contributory to the increased risk of diabetes and CVD in Indians (Yajnik, 2004; Yajnik and Deshmukh, 2012; Yajnik et al., 2003, 2008).

It is now well appreciated that the intra-uterine environment can induce heritable alterations that may be retained over generations (Aiken and Ozanne, 2014; Goodspeed et al., 2015; Ng et al., 2010). In non-human primates, a maternal high-fat diet supplemented with calorically dense treats leading to obesity
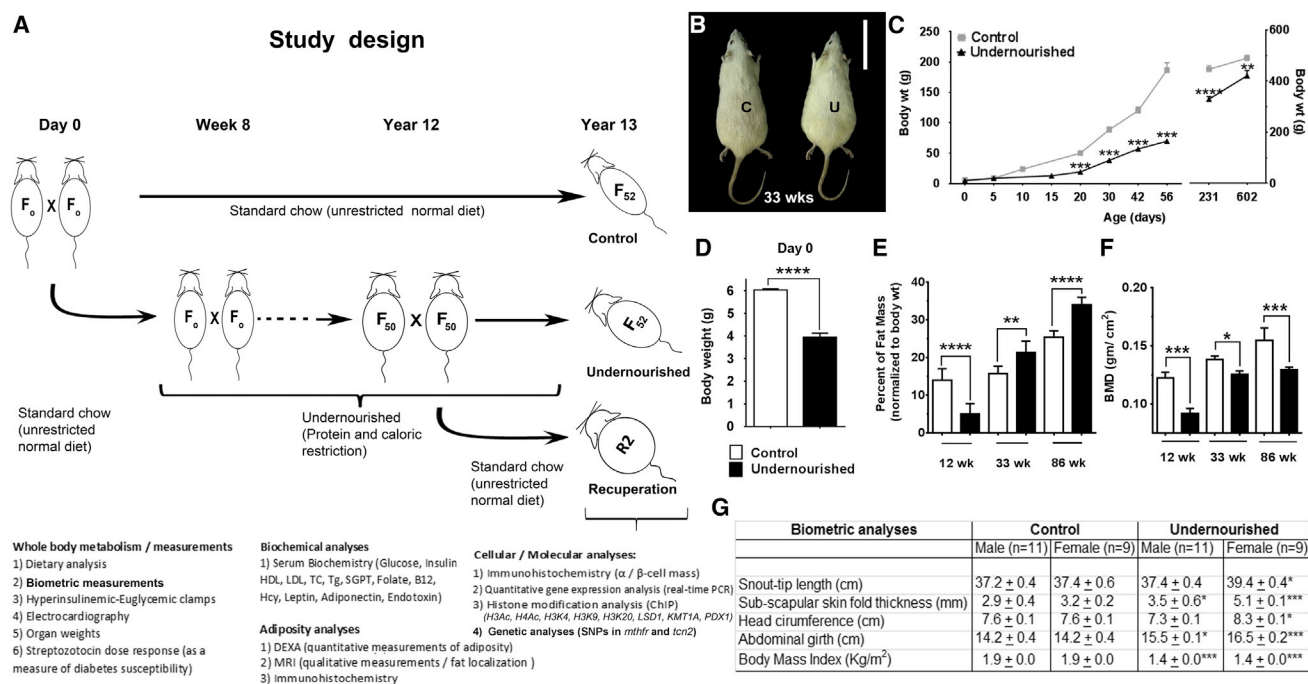
Figure 1. Generation of a Multigenerational Undernourished Rat

(A) Study design illustrating the period of undernutrition and nutrient transition (Recuperation).

(B–F) (B) Control (C) and Undernourished (U) rats; bar, 10 cm, (C) growth curves of Control and multigenerational Undernourished rats showing low birth-weight (D) and no catch-up growth (C), (E) body fat and (F) bone mineral density measured using DXA at 12, 33, or 86 weeks.

(G) biometric measurements in Control and Undernourished rats; n ≥ 8, >4 litters, data presented as mean ± SEM, *p < 0.05, **p < 0.01, ***p < 0.01, and ****p < 0.0001; all comparisons against Controls.

has been shown to epigenetically alter chromatin structure in their progeny via SIRT1-mediated covalent modifications of histones (Aagaard-Tillery et al., 2008; Suter et al., 2012). Increased adiposity and insulin resistance have also been reported in high-fat diet-fed rodent models. Intra-uterine programming may involve epigenetic changes, which can be passed over generations, and may promote the development of adiposity and T2D.

In a preliminary study of naturally occurring food-deprived (for 12 years) Wistar rats, we identified differences in body composition and defects in glucose-insulin metabolism. We therefore decided to study the above phenotype and underlying mechanisms by replicating the diets in this prospective hypothesis-driven study. We present herein the first direct evidence that Wistar rats that are protein calorically undernourished over multiple (50) generations show increased adiposity, insulin resistance, and susceptibility to Streptozotocin (STZ)-induced diabetes. We further demonstrate that this adverse metabolic state is associated with altered histone modification profiles, which cannot be reversed by two generations of nutrient recuperation.

RESULTS AND DISCUSSION

A Multigenerational Rat Model of Undernutrition

Wistar rats were maintained for 50 generations (Figure 1A; Figure S1A) with unrestricted access to standard commercial chow ("Control") or restricted to 50% of ad libitum mass of a chow containing 2.2-fold less protein, 1.3-fold more carbohydrates, 2.1-fold less fat, and 2.4-fold less fiber (Tables S1A, and S1B) with low vitamin supplementation (Table S1C), as compared to Control chow. The Undernourished (U) rats were lighter than Control (C) rats (Figures 1B and 1C), had low birth weight (Figure 1D), and did not show any catchup growth (Figure 1C). Dual-energy X-ray absorptiometry (DXA) measurements demonstrated that Undernourished rats had less body fat (normalized to body weight) than Control rats at 12 weeks of age but increased and exceeded control levels significantly at 33 and 86 weeks of age (Figure 1E). Their bone mineral density (BMD) was lower than Control rats at all times (Figure 1F). Biometric assessment demonstrated increase in skin-fold thickness, abdominal girth, and BMI following multigenerational undernutrition (Figure 1G). Thus, undernutrition over 50 generations led to a phenotype that was lighter at birth, failed to show catchup growth, and demonstrated increasing adiposity later in life.

Attempting to Correct Metabolic Effects of Multigenerational Undernutrition

After 50 generations of undernutrition, Undernourished rats were provided with unrestricted access to a standard (Control) chow diet from day 0 of pregnancy, and their progeny were studied at second generation of recuperation (R2 rats). These rats (Figure 2A) showed restoration of birth weight (Figure 2B, inset; Figures S1B and S1C) to Control values but grew significantly heavier than age-/gender-matched Control rats (Figures 2A
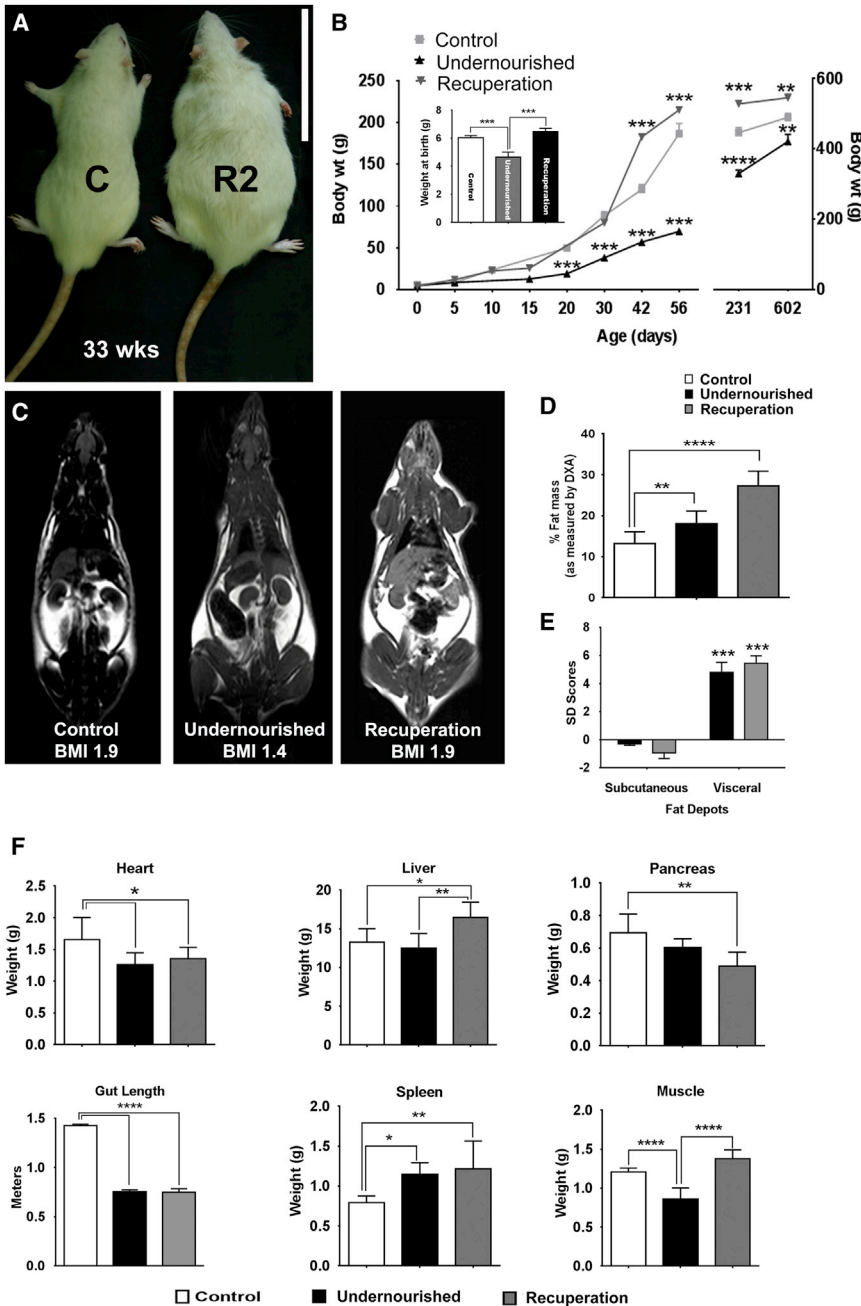
Figure 2. Nutrient Recuperation in a Multigenerational Undernourished Rat

(A and B) (A) Control (C) and second generation Recuperation rat (R2) (B) R2 rats show improvement in birth weight (versus Undernourished; inset in B), but significantly higher body weight postweaning.

(C) MRI for the 33 week Control, Undernourished, and R2 rats; white areas represent fat distribution.

(D and E) (D) Fat mass measured by DXA showed significant increased adiposity in 33-week-old Undernourished and R2 rats, which is (E) mainly visceral (presented as SD scores, relative to Control).

(F) Organ weights of 33-week-old rats (normalized to body weight). Data presented as mean ± SEM, n ≥ 6 (4 litters) (B–F), *p < 0.05, **p < 0.01, ***p < 0.001, and ****p < 0.0001; all comparisons against Controls.

"Thrifty phenotype" hypothesis). However, the adaptive mechanisms of the Undernourished rats were not suited to the changing (Recuperation) environment of unrestricted access to Control chow. Recuperation rats showed restoration of birth weight but heavier body mass, a lighter heart and pancreas, and a heavier liver and spleen compared with Control rats (Figure 2F). Increased hepatic weight was mostly a result of fat accumulation (Figures S2A and S2B), which may contribute to increased splenic weight (Francque et al., 2011; Murray et al., 1986). Brain weight (data not shown) was similar to that in Control rats (both genders). Undernourished rats had smaller muscle mass. Interestingly, the gut length was shorter in Undernourished rats and remained shorter in R2 rats. Protein-deprivation in rats has been shown to lead to shorter intestines (Kasai et al., 2012). Similar changes induced over multiple generations of undernutrition in our study appear to introduce heritable alterations that were not reversed after two generations of "normal" diet. No gender differences were observed (Figures S1B–S1E, S2B, S2G–S2J, S4A, and S4B).

and 2B) after the post-weaning period (Figure 2B; Figures S1D and S1E). Recuperation (R2) rats had higher abdominal girth on day 4 (Figure S1F) and the highest fat mass of the three groups (Control, Undernourished, and Recuperation) at 12 and 33 weeks of age (Figure S1G). MRI identified increased fat deposition in visceral organs of R2 rats, especially the liver (Figure 2C; Movie S1). DXA measurements confirmed significantly higher body fat in Undernourished and Recuperation rats than Controls (Figure 2D), most of which was due to visceral adiposity (Figure 2E). Multigenerational undernutrition thus appears to support mechanisms favoring accumulation of body fat (Stewart et al., 1980; Wells, 2006) as an adaptive mechanism (the so-called

Unrestricted Access to a Control Diet in Multigenerational Undernourished Rats Promotes Adverse Metabolic Health in Later Life

We hypothesized that Undernourished rats provided with unrestricted access to Control commercial chow would present with metabolic profiles that are comparable to Control rats. Undernourished rats (relative to Controls) demonstrated similar circulating concentrations of serum endotoxin (Table S1D) but higher concentrations of circulating glucose (p ≤ 0.01), insulin
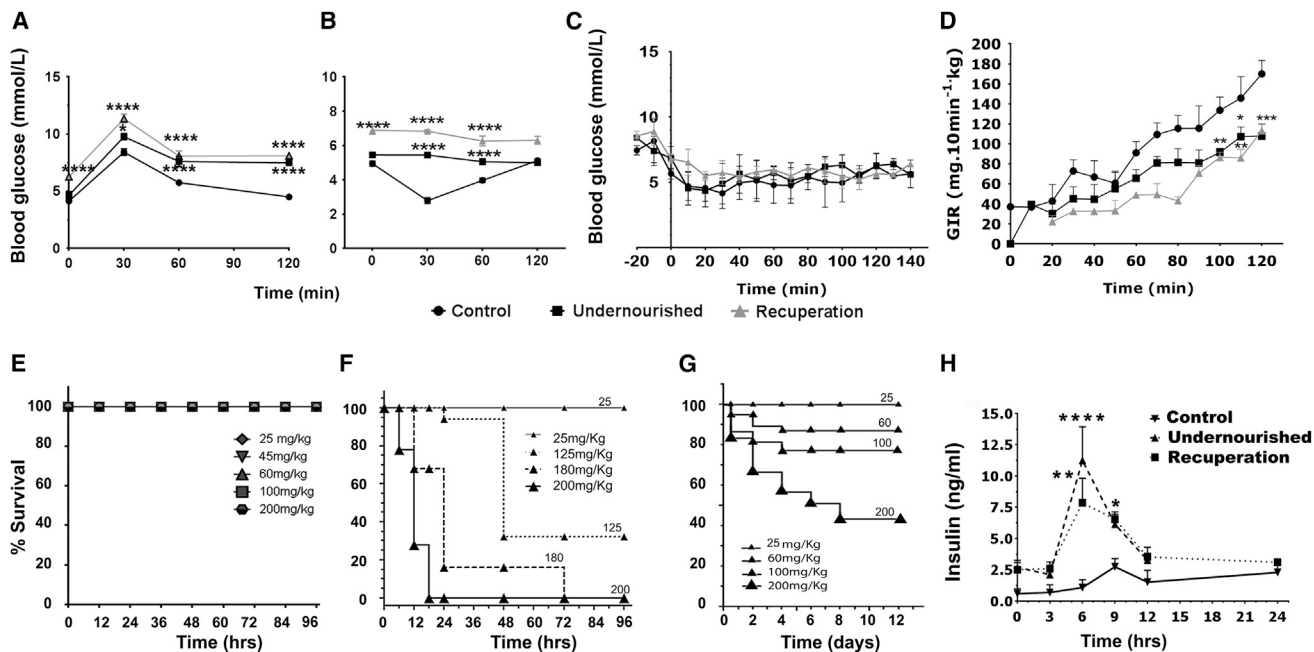
Figure 3. Insulin Sensitivity and Susceptibility to STZ-Induced Diabetes

(A–D) (A) Glucose tolerance test, (B) insulin tolerance test, (C) glucose was clamped during hyperinsulinemic-euglycemic clamp, and (D) glucose infusion rate (GIR) was measured during the clamp.

(E–G) Survival curves for Streptozotocin (STZ) dose response in (E) Control, (F) Undernourished, and (G) R2 rats.

(H) Circulating insulin after STZ injection (200 mg/kg). Data presented as mean ± SD, n ≥ 6 (4–12 litters). (A, B, and E–H) 14- to 20-week-old rats; (C and D) 33-week-old rats; *$p < 0.05$, **$p < 0.01$, ***$p < 0.001$, and ****$p < 0.0001$; all comparisons against Controls.

($p \leq 0.001$), leptin ($p \leq 0.05$), serum glutamic pyruvic transaminase (SGPT; $p \leq 0.001$), total homocysteine (tHcy; $p \leq 0.0001$) triglycerides (TG; $p \leq 0.0001$), and reduced concentrations of high-density lipoprotein-(HDL) cholesterol, folate, and vitamin B_{12} ($p \leq 0.0001$; all). In comparison with Control rats, Recuperation rats demonstrated elevated circulating insulin, glucose ($p \leq 0.0001$; both), leptin ($p \leq 0.001$), endotoxin ($p \leq 0.0001$), TG ($p < 0.0001$), total cholesterol ($p \leq 0.0001$), VLDL-cholesterol ($p \leq 0.0001$), LDL-cholesterol ($p \leq 0.001$), SGPT ($p \leq 0.01$), and tHcy ($p \leq 0.0001$), but similar levels of HDL-cholesterol (Table S1D).

Higher levels of SGPT in Undernourished and R2 rats compared to Control rats was consistent with liver damage due to fat deposition. We also observed that low levels of circulating vitamin B_{12} and folate in Undernourished rats were partially corrected in R2 rats. Macro-nutrient sufficiency thus seems to offer a considerable correction for vitamin B_{12} and folate deficiency as seen in the R2 rats, yet their levels remained significantly lower than Controls. Serum total homocysteine was elevated in Undernourished rats (versus Control) and did not reverse in R2 rats. Recuperation rats were visibly obese (Figure 2A) and showed sedentary habits as compared to Control rats (Movies S2 and S3), despite having similar total energy intake (Table S1B). Higher circulating leptin and lower adiponectin (Table S1D) levels in Undernourished and R2 rats reflected increased adiposity in these rats (Figures 1E and 2D; Figures S1F and S1G). Serum endotoxin concentrations were significantly higher in the R2 rats (Table S1D), as seen in human studies of obese, IGT, and T2D subjects (Harte et al., 2012). Similar to

findings in mouse studies (Smith et al., 1966), elevations in serum endotoxin levels, along with hepatic fat (discussed above), may contribute to heavier spleens (Figure 2F) in Undernourished and R2 rats.

Fasting hyperinsulinemia was a prominent feature of Undernourished and R2 rats although islet insulin content was ~3-fold lower in Undernourished, but not R2, rats (Table S1D). We observed significant increases in numbers of insulin-containing cells in Undernourished and R2 rats with relatively fewer glucagon-containing cells (Figures S2C–S2E), though no significant increases in beta cell mass (Figure S2F) were observed.

Altered Metabolic Health following Multigenerational Undernutrition Is Not Restored through Macronutrient Supplementation

Following assessment of impaired glucose tolerance (Figures 3A and 3B; Figures S2G and S2H), hyperinsulinemic-euglycemic clamp studies were performed on Control, Undernourished, and R2 rats (Figures 3C and 3D; Figures S2I–S2J) to confirm insulin resistance. Significantly lower glucose infusion rates supported maintenance of clamped glucose concentrations in the Undernourished and R2 rats, confirming that the insulin resistance observed in the Undernourished rats was not restored following two generations of Control diet restoration. To understand whether undernutrition over generations altered the susceptibility to diabetes, we carried out a streptozotocin (STZ) dose response (see Experimental Procedures, Figure S3A). STZ, a pancreatic beta cell toxin, is routinely used to induce diabetes in Wistar rats. Undernourished rats died
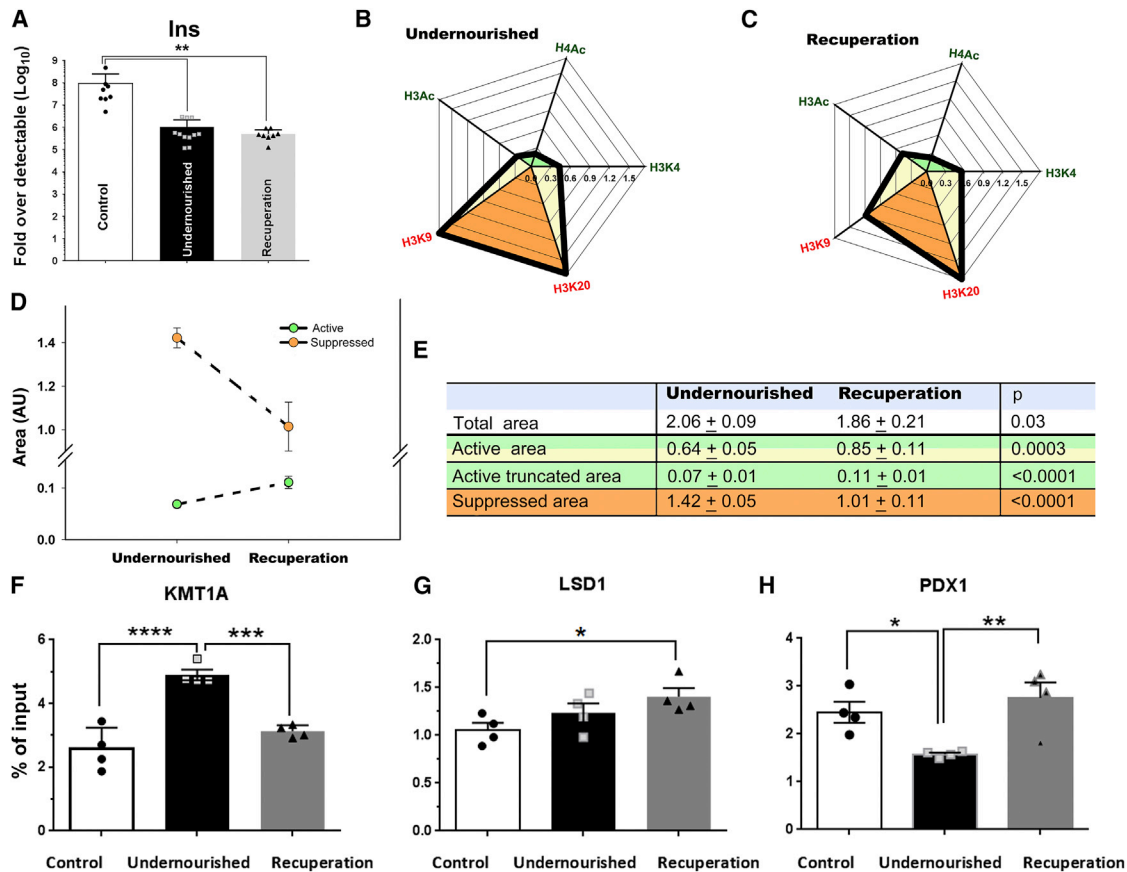
CellPress

Figure 4. Epigenetic Modifications following Multigeneration Undernutrition and Nutrient Transition

(A) Pancreatic Insulin-2 gene transcript abundance.

(B and C) Epigenetic signatures of histone modifications (relative to control, see Experimental Procedures). Areas between the rays of the radar plot were assigned as belonging to "activated" or "suppressed" parts of the epigenetic signature based on the antibodies used for IP. The Shoelace formula was then used to measure the areas of these fragments of the signature. Results were compared using t test and plotted mean ± SD.

(D and E) Areas for "active" and "suppressed" modifications before and after nutrient transition.

(F–H) Recruitment of histone modifying enzymes (F and G) and the transcription factor PDX1 (H) at rat insulin 2 promoter region.

following exposure to a dose of STZ (200 mg/kg b.w.) that rendered ≥90% Control rats (Figure 3E) diabetic (fasting blood glucose > 11 mmol/l by day 8 post-STZ). An 8-fold lower dose (25 mg/kg b.w.) offered 100% survival in Undernourished (Figure 3F) as well as R2 rats (Figure 3G) but all developing diabetes with fasting blood glucose > 11 mmol/l by day 8 from STZ injection; none of the Control animals became diabetic at this (low) dose. We observed that Undernourished and R2 rats injected with this high dose (200 mg/kg b.w.) of STZ died with hypoglycemic convulsions in 12–14 hr (Figures 3F and 3G). Serial circulating insulin measurements following STZ injection (200 mg/kg b.w.) in Undernourished and R2 rats (Figure 3H) demonstrated that the increased mortality at 200 mg/kg dose was indeed associated with a significant increase in circulating insulin within 3–6 hr after STZ injection, which resulted in hypoglycemic convulsions and death. As Undernourished and R2 rats showed 100% survival with fasting plasma glucose > 11 mmol/l by day 8, at a dose that is eight times lower than the diabetogenic dose in Control rats (200 mg/kg b.w), Undernourished and R2 rats had eight times more susceptibility to STZ-induced diabetes.

Undernourished rats also showed other markers of metabolic disorder. Elevated levels of circulating tHcy (Table S1D) is related to higher risk of coronary disease, stroke, and peripheral vascular disease and atherosclerosis in man (Zhou and Austin, 2009). Electrocardiograms (Figures S3B–S3F) revealed inverted P and T waves in R2 rats, with elevated Q and ST-segments, consistent with myocardial infarction and associated with higher early mortality and morbidity (Anderson et al., 2007), in man. A lower circulating concentration of folate (Table S1D) may itself be an atherogenic factor (Imamura et al., 2010) that could promote hyperhomocysteinemia seen in these Undernourished and R2 rats. Cardiac histology revealed multiple morphological abnormalities in R2 rats (Figure S3G) and higher cardiac tissue levels of the DNA methyl transferase *dnmt3a1* in Undernourished and R2 rats (Figure S3H), which may be associated with epigenetic silencing in cardiac tissue as well (Kotini et al., 2011).

Undernourished and R2 rat pancreas contained significantly fewer (pro-)insulin 2 gene transcripts (Figure 4A; Figures S4A and S4B), indicating that multigenerational undernutrition affected insulin gene transcription with no recovery. This may be a result of epigenetic repression of insulin gene transcription,

CellPress

although active degradation of insulin gene transcripts, which have a long half-life (Gershengorn et al., 2004) of ~30–36 hr (in man), or both, is also a possibility. Indeed, the relative abundance of KMT1A, a histone-3 lysine 9-specific methyl transferase, which trimethylates H3K9me leading to suppression of gene transcription (Krauss, 2008; Rai et al., 2006), was increased in Undernourished and R2 pancreas (Figures S4C and S4D). To test whether the pro-insulin gene was epigenetically modified, we carried out chromatin immunoprecipitation (ChIP) for five different histone modifications: H3Ac, H4Ac, and H3K4me3, three modifications associated with transcriptionally activated gene promoters, and H3K9me3 and H3K20me3, two modifications associated with suppressed/silenced gene promoters. TaqMan-based real-time PCR was carried out on immunoprecipitated DNA to quantify the insulin promoter content in each of the IP fractions. Data comparing Undernourished and R2 islets to Control islets (Figure S4E) were logarithmically transformed to create radar plots of the epigenetic signature for insulin promoter (Figures 4B and 4C; Figures S4F and S4G). Areas between the rays of these radar plot were assigned as belonging to "activated" (green) or "suppressed" (orange) profiles and measured to quantify differences in overall epigenetic profiles (Figures 4D and 4E). These analyses demonstrate that epigenetic signatures leading to suppression of pro-insulin gene transcription were markedly increased (relative to Control; Figures S4E–S4H) in Undernourished rat islets and were not restored to Control levels following two generations of unrestricted access to "Control" chow (R2 rats). However, relative to the Undernourished epigenetic profiles, we observed a significant increase in activated marks (p < 0.0001) and a decline in suppressed marks (p < 0.0001) in the R2 epigenetic profile, indicating that two generations of normal feeding, significantly, but only partially, improved epigenetic repressive modifications within the insulin promoter region (Figures 4D and 4E). In order to understand the underlying molecular mechanisms leading to these histone modifications and metabolic alterations, we examined the recruitment of histone modulators and transcription factors at the insulin-2 gene promoter region. H3K9 methyl transferase KMT1A and the corepressor LSD1 were specifically recruited at the insulin gene promoter region in Undernourished and R2 rats, respectively (Figures 4F and 4G; Figures S4I–S4L). Intriguingly, such an epigenetically modified chromosomal conformation significantly diminished the spatial occupancy/recruitment of the pancreatic transcription factor PDX1, at the insulin-2 gene promoter region (Figure 4H; Figures S4I–S4L). These analyses indicate that dietary and lifestyle adaptations/choices are associated with and possibly regulatory in recruiting histone modifying enzymes at the gene promoter region. The overall chromosomal conformation seen in Undernourished rats is inhibitory to efficient binding of the transcription factor PDX1, at the insulin-2 gene promoter region.

Conclusions

The thrifty phenotype hypothesis proposes that type 2 diabetes results from the fetus and the infant having to be nutritionally thrifty, challenging the dogma that type 2 diabetes results from overnutrition in a genetically susceptible individual. The thrifty phenotype idea originated in studies that linked low birth weight with type 2 diabetes but was soon extended to the "thin-fat"

body composition of the fetus and to a metabolic-endocrine profile, which suggested adaptations to tide over poor nutrition during the crucial phase of intrauterine life. Such a phenotype was advantageous if the post-natal nutrition remained poor but led to obesity, insulin resistance, and diabetes in restored food supply. Our multigenerationally undernourished rat model presents with multiple characteristics of multigenerationally deprived human populations of developing countries: low birth weight, thin-fat body composition (central adiposity), insulin resistance, characteristic dyslipidemias, and micronutrient deficiencies of methyl donors. In addition, they demonstrated heightened sensitivity to the diabetogenic doses of STZ. Molecular investigations revealed significant alterations in histone methylation, acetylation, and recruitment of histone modifying enzymes at insulin-2 gene promoter. Overall, differences in chromosomal conformation induced as a result of these modifications led to significant decrease in transcription factor PDX1 binding at the insulin-2 gene promoter. All of these may contribute to altered gene expression observed in the Undernourished rats (Figure S4M). Intriguingly, nutrient recuperation for two generations did not reverse these epigenetic modifications, but rather led to increased obesity and metabolic risk for diabetes with electrocardiographic and histological evidence for cardiovascular disease.

Current investigations failed to show any associations with genetic polymorphisms (data not shown), but further studies are warranted. Our studies have largely focused on assessing the metabolic and epigenetic changes following multigenerational undernutrition and nutrient recuperation. The thrifty genotype hypothesis (Neel, 1999) proposed that increasing prevalence of T2D among populations undergoing nutrient/lifestyle transition resulted from the selection of metabolically thrifty genes. We questioned whether genetic factors are altered during multigenerational undernutrition and whether such changes are reversed by nutrient recuperation. We initiated targeted genetic analyses in the three rat populations. Sequencing of potential SNPs in *mthfr* and *tcn2* genes (associated with cardiac, neural tube, and vitamin B$_{12}$ defects) as well as RNA-sequencing for *Ins-2* transcripts showed no genetic polymorphisms at these loci (data not shown). Future studies involving a desired (40×) coverage through whole-genome sequencing will identify possible contributions of genetic polymorphisms toward metabolic health. Another limitation of the study is that we have assessed metabolic and epigenetic changes following multigenerational undernutrition and relatively short-term (two-generation) nutrient recuperation. Whether nutrient restoration to Undernourished animals for multiple (>2) generations may reverse adverse metabolic effects remains unknown. Another component that would be also interesting to understand is the effect of high-fat diet on Undernourished animals, which would mimic nutrient transition in today's developing countries more accurately.

Additionally, studies involving metagenome sequencing, whole-genome sequencing, and epigenetic profiling in Undernourished, Recuperation, and Control rats during nutrient transition with micronutrient (vitamin B$_{12}$, folate, vitamin B$_6$, magnesium, and vitamin D) supplementation may identify instructive mechanisms that modify our epigenomes during adaptation to a changing diet and lifestyle. The Undernourished

rat model offers unique advantages as a model of a multigenerationally undernourished population then exposed to rapid nutritional and epidemiologic transition, causing a "double burden" of disease. Our model may contribute to the development of a strategy to reduce the mismatch between early- and late-life nutrition and, therefore, facilitate development of newer strategies for diabetes prevention.

EXPERIMENTAL PROCEDURES

Animals
Undernourished rats were derived from a colony of Wistar rats (Control) by feeding a protein caloric-deficient diet (Tables S1A–S1C), as outlined in the study design (Figure 1A). Animals were housed under 12 hr day/night cycle; Control and Recuperation rats were allowed free access to standard commercial chow and water at all times. National and Institutional guidelines for the use and care of laboratory animals were followed. All procedures detailed in this study were approved by the NCCS/NTC Ethics and Animal Welfare Committees. At least 20 litters were used at each generation for propagation of this outbred colony (Figure S1A). Data represent analyses on >6 animals from 4 to 12 different litters.

Biochemical Estimations
Glucose and insulin estimations were carried as detailed in Supplemental Experimental Procedures.

Circulating biomarkers were measured on a Spectrum II Auto analyzer (Abbott Laboratories) as detailed in Supplemental Experimental Procedures.

Dual-energy X-ray absorptiometry (DXA) was carried out on age-matched males at 12, 33, or 86 weeks using Orthometrics p-DEXA scanner. Total/visceral/s.c. fat mass were measured and adiposity were calculated as amount of fat normalized to body weight at the time of measurement.

MRI was performed on age-matched rats using a Siemens 1.5 Tesla machine with 3 mm sections.

Hyperinsulinemic-euglycemic clamp studies were carried out based on the guidelines and procedures detailed by Ayala et al. (2006).

Streptozotocin (STZ), a pancreatic β-cell toxin, was reconstituted in chilled citrate buffer (pH = 4.5) prior to i.p. injection and post-STZ survival was measured as detailed in Supplemental Experimental Procedures.

Immunostaining and confocal microscopy was carried out using methods detailed in Supplemental Experimental Procedures and published earlier (Joglekar et al., 2009).

ChIP and western blotting for epigenetic modulators was carried out as detailed in Supplemental Experimental Procedures.

Quantitative real-time PCR was carried out using SybrG or TaqMan assays as detailed in Supplemental Experimental Procedures. Data are presented as "Fold over detectable" as explained elsewhere (Hardikar et al., 2014).

Statistical Analysis
Differences between groups were calculated by using one-way or two-way ANOVA and appropriate post hoc tests as described in Supplemental Experimental Procedures. SPPS, GraphPad Prism, and Jandel Scientific softwares were used to assess/plot data. A sample size of six rats in each group is sufficient to identify a difference of 27% (SD 15% of mean), with 80% power at $2p = 0.05$ between any two groups, or to identify a difference of 45% (SD 25% of mean) as statistically significant, with 80% power at $2p = 0.05$ between any two groups. Results are expressed as mean ± SEM or SD. SD scores were used to compare organ weights of Undernourished animals in comparison to the Controls. SD score = $\Sigma [(x_i - X_c)/SD_c]$, wherein x_i is individual value in the experimental (Undernourished or Recuperation) group, X_c is the mean value for the Control group, and SD_c is the SD of the Control group. Difference between groups was tested by one-way ANOVA and Fisher's LSD test or Student's t test, as appropriate. Serial changes in plasma glucose and insulin concentrations were tested by paired t test or one-way ANOVA as appropriate. Computations were performed using Graphpad Prism software. Radar plots of the data representing ChIP studies were created by logarithmically transforming fold over detectable data, using shoelace formula.

REFERENCES

Aagaard-Tillery, K.M., Grove, K., Bishop, J., Ke, X., Fu, Q., McKnight, R., and Lane, R.H. (2008). Developmental origins of disease and determinants of chromatin structure: maternal diet modifies the primate fetal epigenome. J. Mol. Endocrinol. 41, 91–102.

Aiken, C.E., and Ozanne, S.E. (2014). Transgenerational developmental programming. Hum. Reprod. Update 20, 63–75.

Anderson, J.L., Adams, C.D., Antman, E.M., Bridges, C.R., Califf, R.M., Casey, D.E., Jr., Chavey, W.E., 2nd, Fesmire, F.M., Hochman, J.S., Levin, T.N., et al.; American College of Cardiology; American Heart Association Task Force on Practice Guidelines (Writing Committee to Revise the 2002 Guidelines for the Management of Patients With Unstable Angina/Non-ST-Elevation Myocardial Infarction); American College of Emergency Physicians; Society for Cardiovascular Angiography and Interventions; Society of Thoracic Surgeons; American Association of Cardiovascular and Pulmonary Rehabilitation; Society for Academic Emergency Medicine (2007). ACC/AHA 2007 guidelines for the management of patients with unstable angina/non-ST-Elevation myocardial infarction: a report of the American College of Cardiology/American Heart Association Task Force on Practice Guidelines (Writing Committee to Revise the 2002 Guidelines for the Management of Patients With Unstable Angina/Non-ST-Elevation Myocardial Infarction) developed in collaboration with the American College of Emergency Physicians, the Society for Cardiovascular Angiography and Interventions, and the Society of Thoracic Surgeons endorsed by the American Association of Cardiovascular and Pulmonary Rehabilitation and the Society for Academic Emergency Medicine. J. Am. Coll. Cardiol. 50, e1–e157.

Ayala, J.E., Bracy, D.P., McGuinness, O.P., and Wasserman, D.H. (2006). Considerations in the design of hyperinsulinemic-euglycemic clamps in the conscious mouse. Diabetes 55, 390–397.

CellPress

Echouffo-Tcheugui, J.B., and Dagogo-Jack, S. (2012). Preventing diabetes mellitus in developing countries. Nat. Rev. Endocrinol. 8, 557–562.

Francque, S., Verrijken, A., Mertens, I., Hubens, G., Van Marck, E., Pelckmans, P., Michielsen, P., and Van Gaal, L. (2011). Visceral adiposity and insulin resistance are independent predictors of the presence of non-cirrhotic NAFLD-related portal hypertension. Int J Obes (Lond) 35, 270–278.

Gershengorn, M.C., Hardikar, A.A., Wei, C., Geras-Raaka, E., Marcus-Samuels, B., and Raaka, B.M. (2004). Epithelial-to-mesenchymal transition generates proliferative human islet precursor cells. Science 306, 2261–2264.

Goodspeed, D., Seferovic, M.D., Holland, W., Mcknight, R.A., Summers, S.A., Branch, D.W., Lane, R.H., and Aagaard, K.M. (2015). Essential nutrient supplementation prevents heritable metabolic disease in multigenerational intrauterine growth-restricted rats. FASEB J. 29, 807–819.

Hardikar, A.A., Farr, R.J., and Joglekar, M.V. (2014). Circulating microRNAs: understanding the limits for quantitative measurement by real-time PCR. J. Am. Heart. Assoc. 3, e000792.

Harte, A.L., Varma, M.C., Tripathi, G., McGee, K.C., Al-Daghri, N.M., Al-Attas, O.S., Sabico, S., O'Hare, J.P., Ceriello, A., Saravanan, P., et al. (2012). High fat intake leads to acute postprandial exposure to circulating endotoxin in type 2 diabetic subjects. Diabetes Care 35, 375–382.

Imamura, A., Murakami, R., Takahashi, R., Cheng, X.W., Numaguchi, Y., Murohara, T., and Okumura, K. (2010). Low folate levels may be an atherogenic factor regardless of homocysteine levels in young healthy nonsmokers. Metabolism 59, 728–733.

Joglekar, M.V., Joglekar, V.M., Joglekar, S.V., and Hardikar, A.A. (2009). Human fetal pancreatic insulin-producing cells proliferate in vitro. J. Endocrinol. 201, 27–36.

Kasai, A., Gama, P., and Alvares, E.P. (2012). Protein restriction inhibits gastric cell proliferation during rat postnatal growth in parallel to ghrelin changes. Nutrition 28, 707–712.

Kotini, A.G., Mpakali, A., and Agalioti, T. (2011). Dnmt3a1 upregulates transcription of distinct genes and targets chromosomal gene clusters for epigenetic silencing in mouse embryonic stem cells. Mol. Cell. Biol. 31, 1577–1592.

Krauss, V. (2008). Glimpses of evolution: heterochromatic histone H3K9 methyltransferases left its marks behind. Genetica 133, 93–106.

Murray, M., Zaluzny, L., and Farrell, G.C. (1986). Drug metabolism in cirrhosis. Selective changes in cytochrome P-450 isozymes in the choline-deficient rat model. Biochem. Pharmacol. 35, 1817–1824.

Neel, J.V. (1999). The "thrifty genotype" in 1998. Nutr. Rev. 57, S2–S9.

Ng, S.F., Lin, R.C., Laybutt, D.R., Barres, R., Owens, J.A., and Morris, M.J. (2010). Chronic high-fat diet in fathers programs β-cell dysfunction in female rat offspring. Nature 467, 963–966.

Rai, K., Nadauld, L.D., Chidester, S., Manos, E.J., James, S.R., Karpf, A.R., Cairns, B.R., and Jones, D.A. (2006). Zebra fish Dnmt1 and Suv39h1 regulate organ-specific terminal differentiation during development. Mol. Cell. Biol. 26, 7077–7085.

Smith, W.W., Brecher, G., Budd, R.A., and Fred, S. (1966). Effects of bacterial endotoxin on the occurrence of spleen colonies in irradiated mice. Radiat. Res. 27, 369–374.

Stewart, R.J., Sheppard, H., Preece, R., and Waterlow, J.C. (1980). The effect of rehabilitation at different stages of development of rats marginally malnourished for ten to twelve generations. Br. J. Nutr. 43, 403–412.

Suter, M.A., Chen, A., Burdine, M.S., Choudhury, M., Harris, R.A., Lane, R.H., Friedman, J.E., Grove, K.L., Tackett, A.J., and Aagaard, K.M. (2012). A maternal high-fat diet modulates fetal SIRT1 histone and protein deacetylase activity in nonhuman primates. FASEB J. 26, 5106–5114.

Wells, J.C. (2006). The evolution of human fatness and susceptibility to obesity: an ethological approach. Biol. Rev. Camb. Philos. Soc. 81, 183–205.

Yajnik, C.S. (2004). Early life origins of insulin resistance and type 2 diabetes in India and other Asian countries. J. Nutr. 134, 205–210.

Yajnik, C.S., and Deshmukh, U.S. (2012). Fetal programming: maternal nutrition and role of one-carbon metabolism. Rev. Endocr. Metab. Disord. 13, 121–127.

Yajnik, C.S., Fall, C.H., Vaidya, U., Pandit, A.N., Bavdekar, A., Bhat, D.S., Osmond, C., Hales, C.N., and Barker, D.J. (1995). Fetal growth and glucose and insulin metabolism in four-year-old Indian children. Diabet. Med. 12, 330–336.

Yajnik, C.S., Fall, C.H., Coyaji, K.J., Hirve, S.S., Rao, S., Barker, D.J., Joglekar, C., and Kellingray, S. (2003). Neonatal anthropometry: the thin-fat Indian baby. The Pune Maternal Nutrition Study. Int. J. Obes. Relat. Metab. Disord. 27, 173–180.

Yajnik, C.S., Deshpande, S.S., Jackson, A.A., Refsum, H., Rao, S., Fisher, D.J., Bhat, D.S., Naik, S.S., Coyaji, K.J., Joglekar, C.V., et al. (2008). Vitamin B12 and folate concentrations during pregnancy and insulin resistance in the offspring: the Pune Maternal Nutrition Study. Diabetologia 51, 29–38.

Yajnik, C.S., Chandak, G.R., Joglekar, C., Katre, P., Bhat, D.S., Singh, S.N., Janipalli, C.S., Refsum, H., Krishnaveni, G., Veena, S., et al. (2014). Maternal homocysteine in pregnancy and offspring birthweight: epidemiological associations and Mendelian randomization analysis. Int. J. Epidemiol. 43, 1487–1497.

Zhou, J., and Austin, R.C. (2009). Contributions of hyperhomocysteinemia to atherosclerosis: Causal relationship and potential mechanisms. Biofactors 35, 120–129.

Multigenerational Undernutrition Increases Susceptibility to Obesity and Diabetes that Is Not Reversed after Dietary Recuperation

Anandwardhan A. Hardikar, Sarang N. Satoor, Mahesh S. Karandikar, Mugdha V. Joglekar, Amrutesh S. Puranik, Wilson Wong, Sandeep Kumar, Amita Limaye, Dattatray S. Bhat, Andrzej Januszewski, Malati R. Umrani, Amaresh K. Ranjan, Kishori Apte, Pranav Yajnik, Ramesh R. Bhonde, Sanjeev Galande, Anthony C. Keech, Alicia J. Jenkins, and Chittaranjan S. Yajnik
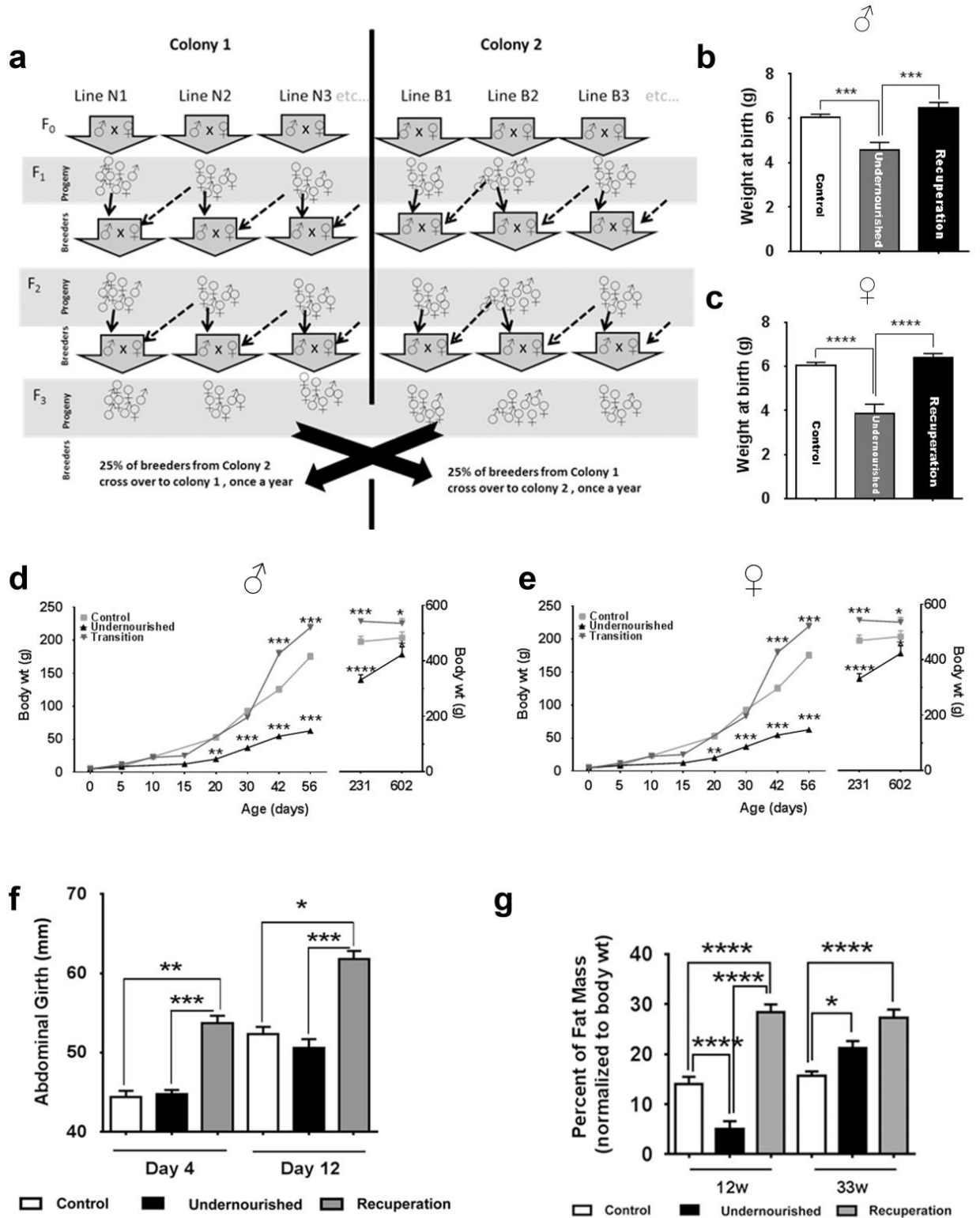
Figure S1

Figure S1, related to Figure 1:

a) In order to avoid any genetic drift in this outbred line, two colonies (Colony 1 and Colony 2) were established at the participating institutions which are geographically separated and managed by different primary animal care takers. Within each of these colonies the following breeding strategy was planned –

i)   Ten to 12 different lines were maintained at a time (N1, N2,N3 etc. & B1, B2 B3 etc…)

ii)   males from one line (within a colony) are used as breeders with females from a different line (within the same colony but a different line).

iii)   males are replaced at every other generation.

iv)   twenty-five percent of the breeding stock was replaced every year with a breeding stock from the other geographically distinct colony (as shown after F_3 above) to maintain the variability achieved through outbreeding. At least 20 different litters were used to propagate the colony in each generation.

b, c) At birth, Undernourished rats were lighter as compared to the Control rats. No differences were seen between males **(b)** and females **(c)** within a group or between birth weights of Control and Recuperation rats. Recuperation rats were significantly heavier than Undernourished rats (both sexes). These data are separate from the animals presented in Figure 1d and 2b (inset) and were obtained by measuring the weights of every rat in the litter and then allocating data to males / females after six days, when identification of their gender was evident. Data presented as mean$\pm$SEM, N=6 rats / group (from four litters), ***p<0.001 and **** p<0.0001; multiple comparisons between groups.

d, e) Growth profiles for the three rat groups broken down based on gender. Data represents body weights from 3-6 rats at each time point, Males and females were not separated/ identified until after six days from birth (4-6 litters). Therefore data for 0 and 5 days represent pooled sets of males and females as their gender was not identified by then. Body weights for 231 and 602 days are plotted on the right Y-axis. Data presented as mean$\pm$SEM, *: p<0.05, **:p<0.01, ***p<0.001 and **** p<0.0001; all comparisons against Controls.

f) Since fat mass estimations could not be carried out prior to 12 weeks of age in the Control rats (limitation of the DXA system used), abdominal girth was measured in day 4 and day 12 litters. Data represent comparison between at least three litters. Recuperation rats showed larger abdominal girth on post-natal day 4, which remained larger on day 12.

g) Adiposity was measured using DXA as described in methods and normalized to body weight for comparing the percent fat mass. Undernourished rats showed lower fat mass at 12 weeks, which increased by over 4-fold in next 21 weeks. Recuperation rats showed higher fat mass at both these time points (12 and 33 weeks). For panels **f** and **g**; N=3 to 8, data presented as mean $\pm$ SEM. *p<0.05, **p<0.01, ***p<0.001 and ****p<0.0001. Gender differences are difficult to identify until day 6 of age and data from panel **(f)** refers to ~1:1 males:females from 4 litters. As discussed earlier, DXA measurements were carried out on males (3-6 litters were analysed). One-way ANOVA, Fisher's LSD comparisons test were used to compare differences between groups.
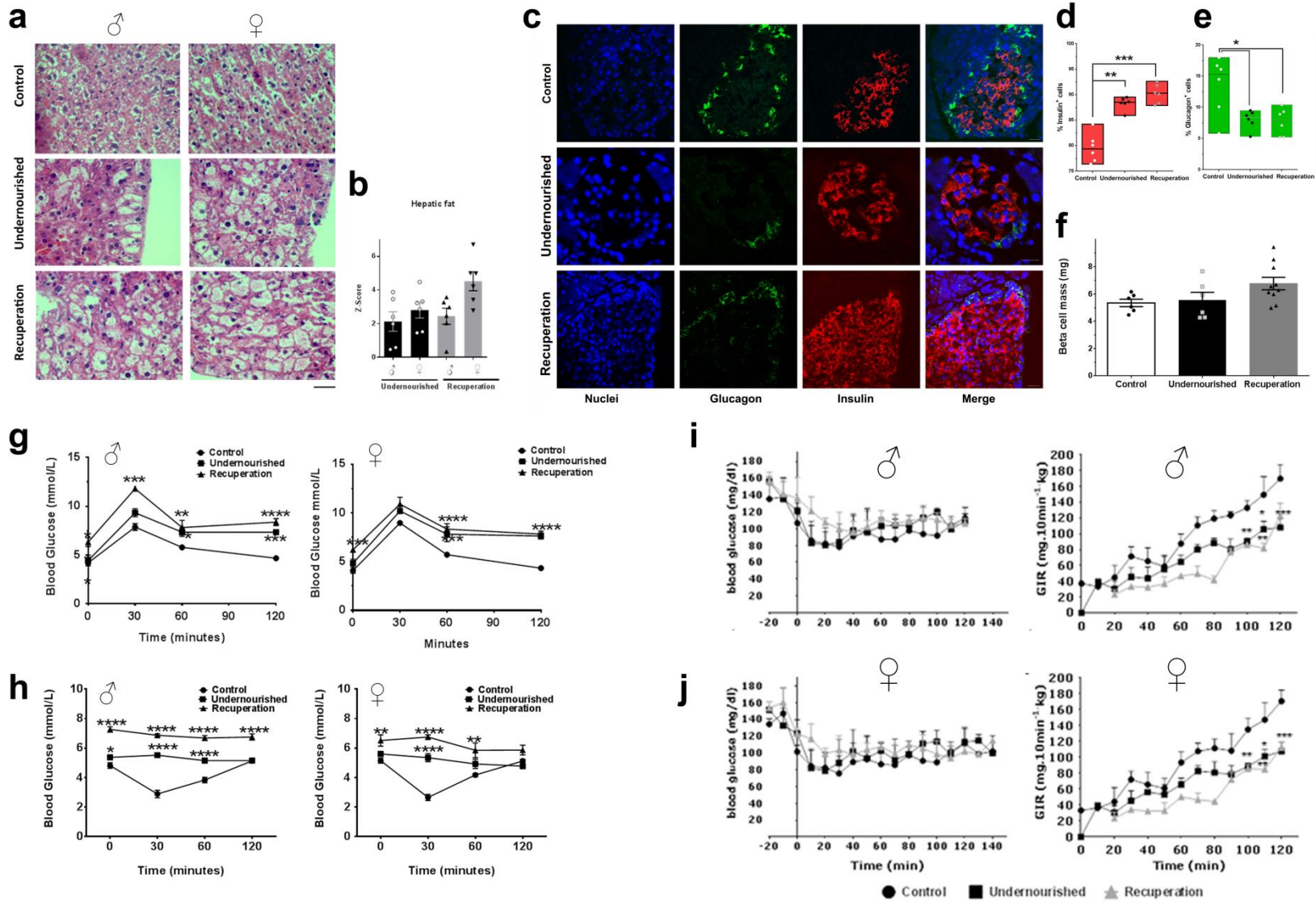
Figure S2

Figure S2, related to Figure 2:

a, b) MRI imaging (Supplemental movie 1 and Figure 2c) indicated that Recuperation rats showed signs of fat deposition in the liver. This was confirmed by comparing liver sections from Undernourished and Recuperation rats to age and gender matched Control rats **(a).** H&E staining shows nuclei in blue and cytoplasm in pink for the 33 week old rats (N=6, 3 males, three litters). The white deposit in the cytoplasm represents fat. Bar represents 25 µm. **(b)** Binary imaging was carried to measure the integrated density of lipid areas and plotted as Z-scores with reference to those in the Control rat liver. Data presented as mean $\pm$ SEM.

c-e) Immunohistochemistry analysis of insulin- and glucagon-producing cells in 33-week old rats. **(c)** No major differences in the islet architecture (localization of Glucagon- Vs Insulin-producing cells within the islet) were observed between Control, Undernourished and Recuperation islets. Bar represents 25µm. Undernourished and Recuperation islets had more Insulin-producing cells **(d)** and fewer Glucagon-producing cells **(e)**. Data presented as mean $\pm$ SEM. $*p \leq 0.05$, $**p \leq 0.01$ and $***p \leq 0.001$ from measurements made using at least 15 different pancreas sections each and from 3 to 6 pancreas – each from a different litter, spaced at 150µm.

f) To assess if changes in beta cell number (Figure S2c,d) led to an increase in beta cell mass, we measured the mass of insulin-producing beta cells in 12-week old rats (N=6-10; 3-5 males, four litters). No differences were seen across groups, nor were any gender differences seen between groups. Further studies assessing serial measurements of beta cell mass during the life course of these rats and after nutrient transition will help understand if nutrient changes alter beta cell fraction, beta cell mass or beta cell number (Chintinne et al., 2012) during their life.

g, h) Plasma glucose concentrations were measured in overnight fasted Control, Undernourished and Recuperation rats during a glucose tolerance test **(g)** (intraperitoneal glucose at 2g/Kg body weight). Circulating glucose concentrations were measured in overnight fasted Control, Undernourished and Recuperation rats after intra-peritoneal insulin (0.15U/Kg) injection **(h).** N=8, four males in each group and representing four different litters from 20 week old rats. For panels f, g and h, data are presented as mean$\pm$SEM, $*$: $p < 0.05$, $**$:$p < 0.01$, $***p < 0.001$ and $****$ $p < 0.0001$; all comparisons against Controls using two-way ANOVA.

i, j) Insulin resistance observed during glucose and insulin tolerance tests was confirmed by carrying out hyperinsulinemic euglycemic clamps (Figure 3c,d). Data from at least 3 or 4 males **(i)** and an equal number of females **(j)** for each of the three groups (Control, Undernourished and Recuperation) were assessed - no significant gender differences were seen in terms of insulin resistance observed in the Undernourished and Recuperation rats. Data presented as mean$\pm$SEM, 33-week old rats and a total of four litters. * $p<0.05$, ** $p<0.01$ ***$p<0.001$ and **** $p<0.0001$; both experimental groups compared to Controls.

Figure S3
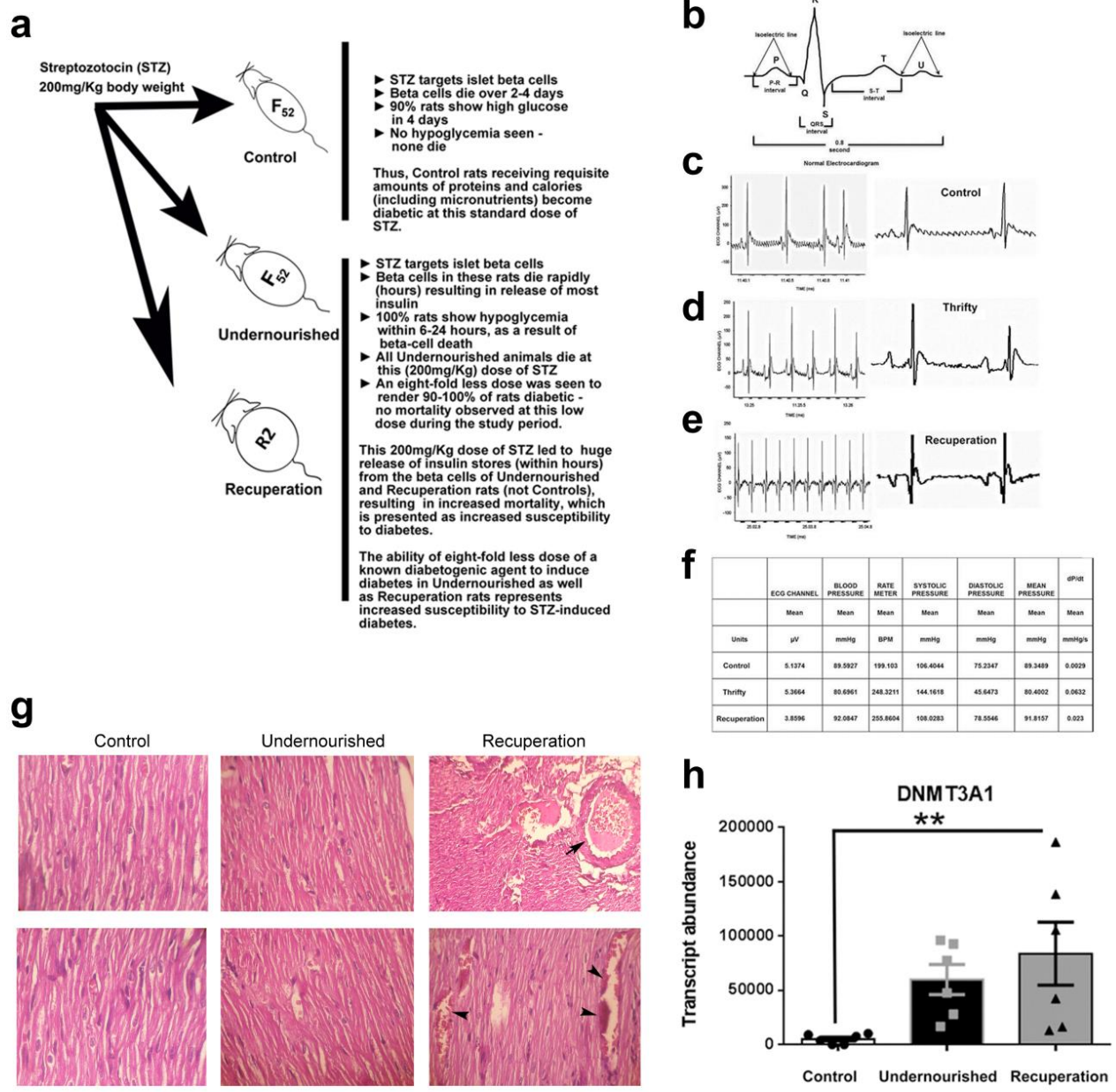
Figure S3, related to Figure 3:

a) Streptozotocin (STZ), a common diabetogenic agent, rendered at least 90% of the Control rats diabetic (without any death) when injected i.p, at a dose of 200mg/Kg body weight. However, this same dose of STZ caused massive release of insulin stores from dead and dying pancreatic beta cells of Undernourished and Recuperation rats, leading to hypoglycemic coma and death within hours of STZ injection. The dose of STZ had to be reduced by eight fold (25mg/Kg body weight) after which, almost all Undernourished and

over 90% Recuperation rats become diabetic. The potential of this lower dose of STZ causing beta cell death and diabetes was measured in terms of survival (Figure 3e-g) after STZ injection and represents increased susceptibility to STZ-induced diabetes.

b-f) Cartoon showing an example of a normal EKG **(b)**, **(c)** EKG of Control rats showing normal EKG pattern, **(d)** Undernourished rat EKG showed raised 'P' and 'T' waves with irregular 'R' and 'S' wave pattern, **(e)** Electrocardiogram of Recuperation rats showed inverted 'P' and 'T' waves with elevated Q and ST-segments, as normally seen with myocardial infarction and associated with higher early mortality and morbidity, and **(f)** EKG table summarizing several cardiac parameters in Control, Undernourished and Recuperation rats. Data are presented as mean values of N=3 to 5 rats for each group, three males and from four litters at 33 weeks of age.

g) Hearts from four to eight Control, Undernourished and Recuperation rats (50% males, four litters) at 14-16 weeks of age were isolated, fixed in paraformaldehyde, sectioned and stained with Haematoxylin and Eosin. No histological abnormalities were seen in any of the Control or Undernourished hearts at this age, but vascular congestion (arrowheads) and atrial thrombus (arrow) were seen in Recuperation rat hearts. Bar=10μm.

h) The levels of DNA methyltransferase gene (*dnmt3a1*) transcript was assessed using TaqMan-real time PCR and found to be significantly increased in cardiac tissue of Recuperation rats. N=6, three males, four litters, 33-week old, data presented as mean $\pm$ SEM. **$p \leq 0.01$, One-way ANOVA, Fisher's LSD comparisons test was used to compare differences between groups.

Figure S4

Group	Total area	Active area	Active truncated area	Supressed area
Undernourished 1	2.17	0.68	0.08	1.50
Undernourished 2	2.16	0.71	0.08	1.45
Undernourished 3	2.13	0.69	0.08	1.45
Undernourished 4	2.12	0.68	0.08	1.44
Recuperation 1	1.99	0.84	0.10	1.15
Recuperation 2	2.16	1.03	0.13	1.14
Recuperation 3	2.07	0.99	0.13	1.09
Recuperation 4	2.03	0.93	0.12	1.10
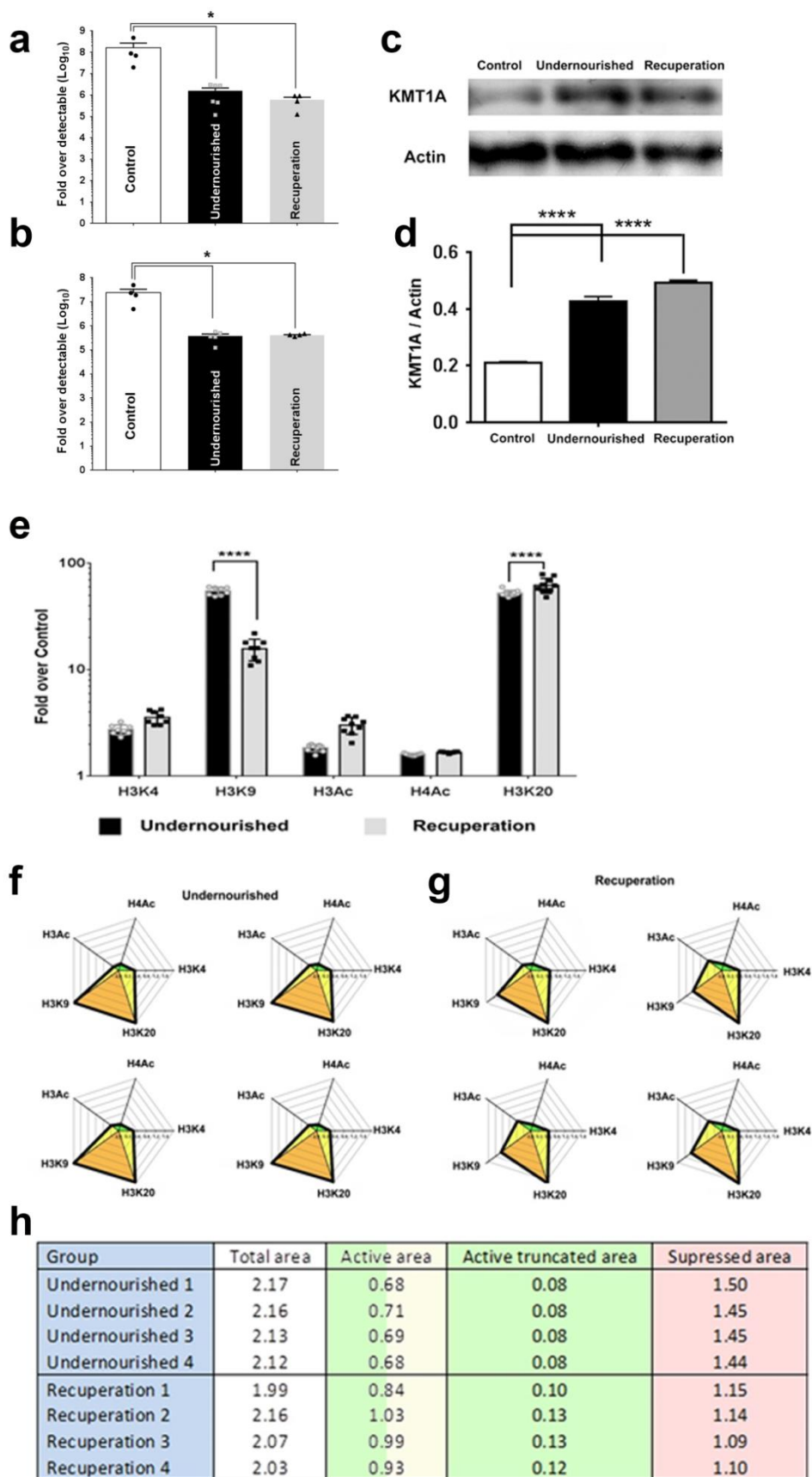
Figure S4, related to Figure 4:

a, b) Transcript abundance of *ins-2* gene was assessed using TaqMan-based real-time PCR in pancreas from Control, Undernourished and Recuperation rats. Insulin gene transcripts were ~100-fold lower in abundance in Undernourished rats with no change following Recuperation. These differences were seen in both males **(a)** and females **(b)** across the groups; no differences observed between males and females within each of the three groups. Each of the points in the overlay scatter plot represents a different pancreas sample from a different rat. Data represents rats from four different litters at 33 weeks of age. Data presented as mean $\pm$ SEM, *: $p<0.05$.

c, d) The expression of histone methyl transferase (KMT1A) was assessed in the pancreas of 33-week-old Control, Undernourished and Recuperation rats. A representative western blot showing abundance of KMT1A in the pancreas of Control (lane 1; left), Undernourished (lane 2) and Recuperation (lane 3) rats **(c)** is shown. Actin was probed as a housekeeping control. Quantitation of blots from six different rats (three males, total of four litters) indicates that the Undernourished and Recuperation rats had increased abundance of KMT1A in the pancreas as compared to those in the Control rats **(d)**. Data presented as mean $\pm$ SEM. ****$p<0.0001$, one-way ANOVA, Fisher's LSD comparisons test was used to compare differences between groups.
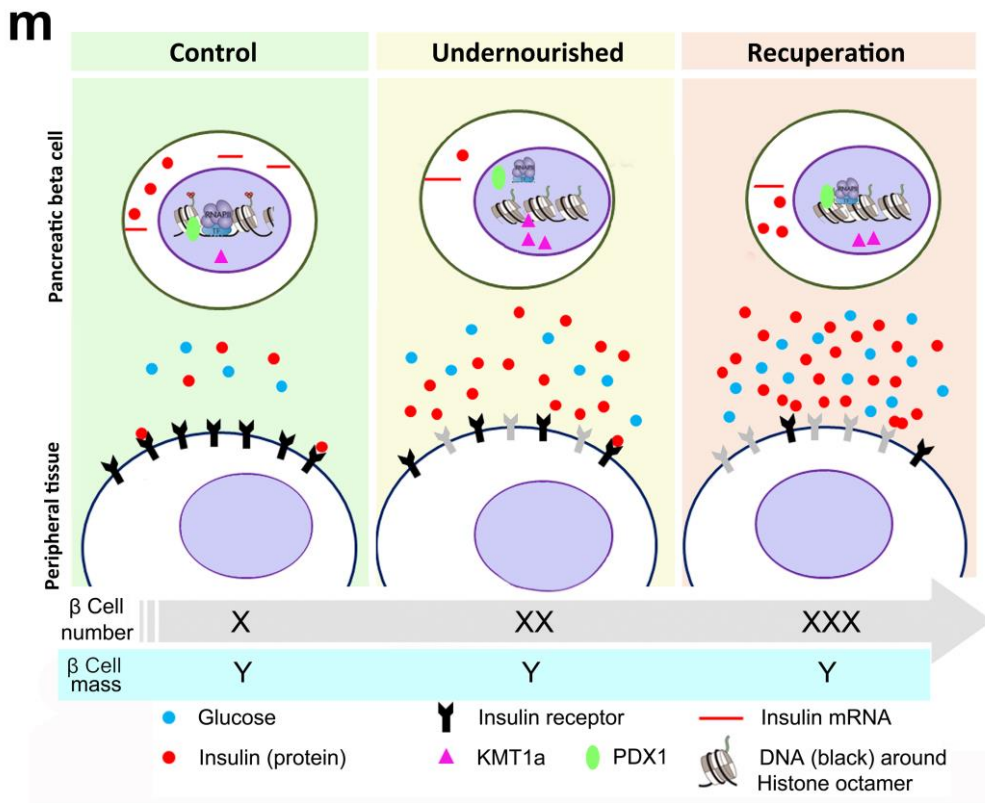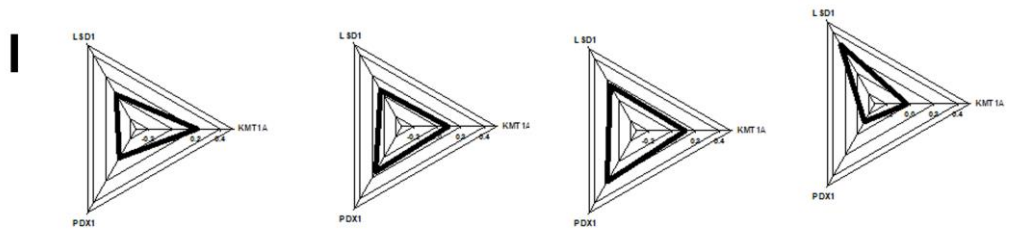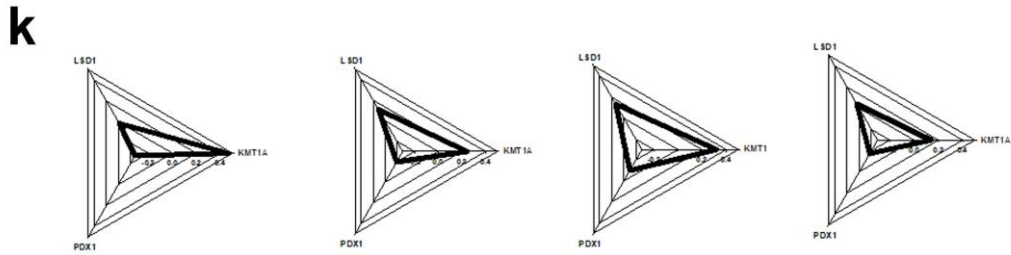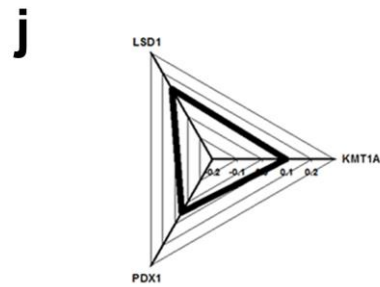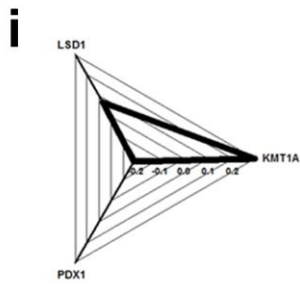
e-h) Chromatin immunoprecipitation (ChIP) for five different histone modifications was carried out on islet cells isolated from Control, Undernourished and Recuperation rat pancreas and data are presented as fold relative to those in the Control rat pancreatic islets **(e)**. Data are presented as mean $\pm$ SEM (N=8 to 9, 33 week old, four males, and from four litters ****$p\leq0.0001$). Data from ChIP studies (shown in panel e, above) were logarithmically transformed and values were used to create radar plots of epigenetic signatures/profiles. Panels **(f)** and **(g)** present individual log transformed data from four of the eight rats used in panel e (above). Data from individual samples are plotted so as to demonstrate the low variability (within a group and across the four litters) seen in the signature/profile (as opposed to individual histone modification shown in panel "e" above) of these five different histone modifications in each of the four rat pancreatic islets. Areas between the rays of the radar plot were assigned as belonging to "activated" (green color) or "supressed" (orange color) parts of the signature based on the effect of specific histone modification. The Shoelace formula was then used to measure the areas belonging to "activated" or "suppressed" signature. Results were compared using t-test. **h)** table

representing the actual areas for signatures of "active" (labelled as Active truncated area) and "suppressed" (labelled as Supressed area) gene promoters in each of the four Undernourished and Recuperation rats shown in panel f and g. The area tabulated as 'Active area' is the sum of the green and yellow areas (from radar plots) and represents the sum of areas for the activated modifications (from H3Ac to H3K4 through H4Ac) as well as the areas between activated and suppressed regions (yellow region between H3Ac to H3K9 and between H3K4 to H3K20).

i-l) Pancreas from 33-week old rats (n=6, three males, four litters) were taken for islet isolation. Islet cells were cross-linked and processed for Chromatin immunoprecipitation using protocol described herein. Two of the samples (one of each gender) had to be pooled at the post-clearing stage due to low amounts of immunoprecipitated DNA. Immunoprecipitation was carried out for the epigenetic modulators LSD1 and KMT1a as well as the pancreatic homeobox gene 1 protein PDX1. Following immunoprecipitation and DNA isolation, real-time PCR was carried out using primers targeting the *ins-2* gene promoter region so as to find out recruitment of these epigenetic modulators and the transcription factor PDX1 at the insulin gene promoter region. Panels **(i)** and **(j)** present radar plots for Undernourished and Recuperation rats respectively (presented as mean of all values). Panels **(k)** and **(l)** present the radar plots for four of the Undernourished and Recuperation individual rat(s) respectively.

m) We demonstrate that Wistar rats that are fed a diet that not only provides lower amounts of protein but also fewer calories and most importantly, inadequate micronutrients, impacts epigenetic mechanisms resulting in significant metabolic defects.

At a cellular level, Undernourished and Recuperation rats showed higher levels of H3K9 methylation in the pancreas as well as increased recruitment of KMT1a at insulin gene promoter in Undernourished rats. KMT1a and LSD1 confer repressive epigenetic conformation that possibly limits the transcription efficiency (as represented in this cartoon by the binding of RNAPII and PDX1 to *ins-2* gene promoter region) leading to significantly lower levels of pro-insulin mRNA in the cells.

Any improvement in activated / repressed epigenetic marks at insulin gene promoter region seen in Recuperation rats may be responsible for increase in islet insulin content (possibly through efficient translation or other mechanisms currently unknown). Undernourished and Recuperation rats show insulin resistance (Figure 3A-D) as represented by a non-functional (grey colour) insulin receptor on peripheral cells, resulting in higher circulating glucose and therefore higher insulin concentrations.

Table S1

a) Dietary analysis: Percent of mass

	Dietary Parameters	Control chow (%)	Undernourished chow (%)	Fold Difference (Control chow Vs Undernourished chow)
1	Moisture	13.0	36.2	2.8
2	Protein	20.0	9.0	-2.2
3	Carbohydrates	26.5	35.5	1.3
4	Fat	4.0	1.9	-2.1
5	Fiber	32.5	13.6	-2.4
6	Ash	4.0	3.8	-1.0

b) Energy (kJoules/Kg/day)

	Dietary Parameters	Control (C)	Undernourished (U)	Fold difference (C Vs U)
1	Protein	66.9	15.1	-4.4
2	Carbohydrates	88.7	17.5	-5.1
3	Fat	30.1	14.5	-2.1

c) Nutrient analysis of Control and Undernourished diet

	Dietary analysis	Control chow ("Commercial" chow, units per 50g of feed)	Undernourished chow ("Customized" feed, units per 50g of feed)
1	Vitamin A	0.0075 IU	0.00524 IU
2	Vitamin D3	0.002 IU	-
3	Vitamin E	5.0 IU	0.055 IU
4	Vitamin K3	1.5 ppm	0.000091ppm
5	Vitamin B1	2.5 g	0.0085 g
6	Vitamin B2	6.0 g	0.055 g
7	Niacin	15.0 g	0.164 g
8	calcium pantothenate	7.5 g	0.0265 g
9	Vitamin B6	2.5 g	0.010 g
10	Vitamin B12	0.0750 g	-
11	Folic acid	1 g	-
12	Biotin	0.100 g	-

d) Serum biochemistry

Parameters assessed	Control (C)		Undernourished (U)		Recuperation (R2)	
	Mean	SD	Mean	SD	Mean	SD
Biometry						
Birth Weight (g)	6.03	0.1	4.3****	0.5	6.0	0.3
Body Weight (g)	454.2	12.9	395.4***	14.3	531.7***	14.8
Glucose-Insulin metabolism						
Glucose(mmol/l)	5.0	0.6	5.7**	0.2	7.2****	0.1
cInsulin (ng/ml)	0.6	0.1	0.9****	0.3	2.9****	0.5
iInsulin (ng/μg protein)	1.6	0.1	0.5*	0.0	1.5	0.1
Whole body metabolism						
Total Fat (%)	13.2	2.9	18.1**	3.1	27.3****	3.6
Leptin (ng/ml)	3.9	1.8	9.2*	3.6	15.2***	5.6
Adiponecin (μg/ml)	22.4	7.2	11.3***	2.7	16.1*	2.4
Endotoxin (EU/ml)	4.3	0.7	6.3	0.9	13.8****	3.7
TG (mg/dl)	59.9	1.8	84.9****	3.8	93.2****	10.4
Total cholesterol(mg/dl)	54.4	0.9	46.0****	2.4	70.1****	2.1
HDL (mg/dl)	21.2	1.1	12.6****	2.0	21.6	3.5
VLDL (mg/dl)	12.0	0.4	17.0****	0.8	18.6****	2.1
LDL (mg/dl)	21.2	1.5	16.4*	1.7	29.9***	4.4
SGPT (IU/liter)	28.4	5.8	72.0***	23.9	58.3**	10.7
Folate (nM/l)	95.7	5.5	44.7****	5.7	83.1***	1.6
Vitamin B12 (pM/l)	851.8	96.0	442.4****	21.8	736.3*	42.2
tHcy (μM/l)	4.6	0.8	10.1****	1.2	13.8****	0.8
Cardiac profile						
Systolic BP (mmHg)	106.0	14.0	140.0*	11.0	108.0	12.0
Diastolic BP (mmHg)	75.2	5.0	45.6**	8.3	78.6	12.0
Heart rate (beats/min)	199.0	22.0	248.0*	15.0	255.0*	25.0

Table S1, related to Figure 1 and 2: Dietary and serum biochemical analysis.

a) Nutrient analysis of Control and Undernourished diet: The chow of Control (or Recuperation) as well as Undernourished rats were analyzed by an independent National Food Analysis Laboratory. Control (standard) chow was low in moisture and carbohydrates content as compared to the Undernourished chow and had higher protein and fiber content. The fat content of Undernourished chow was half the content in Control chow. The amount of Control chow consumed by the Control rats was estimated through a pilot study using metabolic cages. Rats from the Undernourished group received daily chow that was equivalent to 50% (10 grams) of the food mass consumed by Control rats (~20grams) per

day. **b)** Since carbohydrates, proteins and fats together constitute 100% of dietary energy, the net % reduction in total calories was 2.1-times less and the protein was 4.4-times less than those in the control diet. The source and complexity of carbohydrate (starch) was the same in both the diets. **c)** Dietary analysis was carried out by assessment of actual food constituents of the Undernourished rat chow by an independent analytical laboratory (VRK Nutritional Solutions, Pune, India). The values for micronutrients in the control diet were significantly higher in the Control rat chow and were obtained directly from the commercial feed (chow) provider. **d)** Serum biochemistry of Control, Undernourished and Recuperation (R2) rats at 33 weeks of age. Age and gender matched Control rats were compared with Undernourished and Recuperation (R2) rats for biometric, biochemical and metabolic profiles. "c" in the table refers to "circulating" insulin, while "i" in the table refers to "islet" insulin. Data are presented as mean $\pm$ SD. *p<0.05, **p<0.01, ***p<0.001 and ****p<0.0001, n $\geq$ 6 ($\geq$4 litters) in each group; all comparisons against Controls.

Supplemental movie legends

Supplemental Online Movie 1, related to Figure 2: Localization of fat depots in the Recuperation rats

Recuperation rats (normal Wistar rats undernourished for 50 generations and then examined after two generations of unrestricted access to Control chow) showed significant increase in adiposity (Figure 2C-E, Figure S1f,g). This movie demonstrates the localized deposition of adipose tissue using MRI while the rat is scanned from dorsal to ventral side. All adipose tissue appears white in color on MRI – note the fatty deposition in liver, which is confirmed by immunostaining in Figure S2a,b.

Supplemental Online Movie 2, related to Figure 1: Control rats

Control chow fed Wistar rats visualized during mid-day. Control rats were typically active and showed the usual exploratory behavior in the day. Note they also appeared leaner than the Recuperation rats (Supplemental online movie 3).

Supplemental Online Movie 3, related to Figure 2: Recuperation rats

Recuperation rats (normal Wistar rats undernourished for 50 generations and then examined after two generations of unrestricted access to Control chow) appeared obese as compared to the Control rats (Supplemental movie 2) and did not show any significant activity during mid-day. The image capture and playback settings for this movie are identical to that of the Control animals (Supplemental online movie 2).

Supplemental experimental procedures

Animals: Normal Wistar rats were fed a standard commercial chow diet for up to 52 generations (Control rats) or provided 50% restricted (by mass) low protein and high carbohydrate specialty chow (Undernourished rats; see Table S1a-c). In order to assess the metabolic effects of nutrient transition, undernourished rats after 50 generations of protein-caloric undernutrition were transferred on to the normal (Control) chow diet and given food and water ad libitum from day 0 of pregnancy (Day of mating is calculated as Day 0 of pregnancy. When a vaginal plug is confirmed in the breeding female, this is noted as Day 0.5 of pregnancy). For reasons unknown to us as yet, we found that the first generation of Recuperation rats (R1) showed significantly smaller litter size (data not shown) and we had to use these low numbers of R1 rats to set up the breeding pairs for the second generation of Recuperation rats (R2). Therefore all studies were carried out on the second generation of these Recuperation rats (R2 rats; Figure 2) and are presented throughout this manuscript. In order to avoid any genetic drift in this outbred line, two colonies (Colony 1 and Colony 2) were established at the participating institutions which are geographically separated and managed by different primary animal care takers (Figure S1a).

 The breeding strategy is illustrated in Figure S1a and was planned such that
   i) Ten to 12 different lines were maintained at a time (N1, N2,N3 etc & B1, B2 B3 etc…)
   ii) males from one line (within a colony) are used as breeders with females from a different line (within the same colony).
   iii) males are replaced at every other generation.
   iv) twenty-five percent of the breeding stock was replaced every year with a breeding stock from the other geographically distinct colony (see Figure S1a) to maintain the variability achieved through outbreeding.

Although these strategies can maintain variability, we recognize that commercial vendors would maintain over 200 such lines, which was not possible for us in an academic setting. It can therefore be argued that a potential genetic drift may be introduced through the breeding process wherein certain alleles may be selected and be the underlying cause of the metabolic

defects observed in our Undernourished and Recuperation rat colonies. Although preliminary analysis targeting MTHFR and TCN2 gene loci does not indicate any differences in gene sequence, one of the limitations of the present study is that whole genomic sequencing of rats from the three groups (Control, Undernourished and Recuperation), is not available. Although such data can be obtained at lower (~4X) coverage of the genome, these will not be conclusive due to the resolution offered at that coverage. A desired (40X) coverage in whole genome sequencing, will form part of a future study that is planned for the coming year.

Control rats are housed under standard conditions and allowed free access to standard rat chow and water at all times. The mass of daily feed consumed by the Control rats was measured in a pilot study using metabolic cages and 50% restriction of calories was introduced in the Undernourished rats so as to mimic the protein-caloric undernutrition often seen in countries from the developing world. Recuperation rats were maintained on the Control chow and under the exact same conditions as for the Control rats. Animals are housed under 12 hour day / night cycle. Institutional guidelines for the use and care of laboratory animals are followed at all times. The procedures detailed in this study were approved by the NCCS/NTC Ethics and Animal Welfare Committees and access provided as per the ICMR/ Government of India guidelines on the use of laboratory animals.

Dietary intake and body composition:

All measurements for food intake were carried out using metabolic cages (Harvard Apparatus, Holliston, MA). The chow of Control (and Recuperation) as well as Undernourished animals was analyzed by an independent National Food Analysis Laboratory and presented after normalization to the mean weight of chow consumed by Control or Undernourished rats (Table S1a-c). Dietary micronutrient analysis was carried out by assessment of actual food constituents of the Undernourished chow by an independent analytical laboratory (VRK Nutritional Solutions, Pune, India). The micronutrient values for Control chow were obtained directly from the provider (Table S1c). The dietary intake for Undernourished rats was decided at the onset of the study. No significant change was observed in the dietary intake of Control rats over the 52 generations.

Biometric measurements:

Animals (n=6 to 8) were sedated with isoflurane and weighed on an electronic balance (BL6205, Shimadzu Corp., Japan; least count (LC) 0.01 g). Length was measured from tip of

the snout to tip of the tail in a 'relaxed' posture with a non-stretchable tape (John Bull, London, UK). Since the length is dependent on skeletal development, (including the development of caudal vertebrae), we measured total length as that from snout to tip of the tail. Measurement of tail length along with snout to rump length has been described earlier (Hughes and Tanner, 1970). Head circumference was measured at a standardized point just behind the ear base. Skin-fold thickness was measured on the back (caudal to the ribcage) with Harpenden calipers (John Bull, London, UK). Abdominal girth (an index of 'central adiposity') was measured above the hind limbs (Figure 1G, S1f). Three observers carried out all measurements presented in this study ($c.v <3$ %).

***Biochemical estimations*:**

The individual biochemical estimations were performed using at least 6 samples from each group (Table S1d).

Glucose and insulin estimations: Plasma glucose was estimated by a glucose oxidase method using Analox GM7 analyser (Analox Instruments, London, UK) and calibration standards from Sigma, Dorset, UK or by using a blood glucose meter (Accu-Chek, Roche Diagnostics, India), during clamp studies. Serum insulin concentrations were measured by using an ELISA kit (Linco Research Inc, USA).

Circulating biomarkers: Total cholesterol, HDL-cholesterol and triglycerides were measured in fasting animals from each group on a Spectrum II Auto analyzer (Abbott Laboratories, Texas, USA) using standard kits (Sigma-Aldrich, Diagnostic Division, Dorset, UK). Homocystein was measured using HPLC as described earlier (Puranik et al., 2011). Leptin and Adiponectin were measured using ELISA kits from Abcam.

Lifespan of Undernourished rats:

We observed that Undernourished animals had a life span of 22 to 30 months. Control rats had a life span of 32-38 months.

Dual-energy X-ray absorptiometry (DXA):

DXA scans were carried out on age and sex matched animals of 12, 33 or 86 weeks (n=6 to 8 males) using Orthometrics p-DEXA scanner. Total/visceral/s.c. fat mass measured and adiposity is calculated as amount of fat normalized to body weight at the time of measurement.

Magnetic resonance imaging (MRI):

MRI was performed on age matched rats using a Siemens 1.5 Tesla machine with 3mm sections.

Organ weights:

At least six to eight males at 33 weeks age from each group were anaesthetized and dissected to remove brain, heart, liver, pancreas, spleen and muscle. All organs were immediately weighed on a balance Shimadzu Corp., Japan; after blotting off excess water from their surface. Biceps and triceps muscles of the left forelimb were removed and weighed.

Blood sampling:

Fasting blood samples were obtained by retro-orbital puncture under isoflurane anesthesia in EDTA containing vacutainers. Samples were centrifuged at 4000 rpm for 15 min and plasma was stored at -80°C until assayed. Similarly an aliquot was collected in nuclease free sterile tubes and the samples were centrifuged at 4000 rpm for 15 min and serum samples were stored at -80°C until assayed.

Tolerance tests:

Glucose and insulin tolerance tests were carried out in fasted rats. All animals were bled at the start of the tests. For glucose tolerance test, glucose was intra-peritoneally injected at a dose of 2g/Kg body weight and blood glucose concentrations measured at 30-, 60- or 90-minutes after the glucose load. For insulin tolerance test, rats were intra-peritoneally injected with 0.15U/Kg body weight soluble insulin (Human Actrapid, Novo Nordisk, India) and serial glucose concentrations measured.

Hyperinsulinemic-euglycemic clamp studies:

All clamps were carried out based on the guidelines and procedures detailed by Ayala J et al (Ayala et al., 2006). Briefly, all animals were fasted for 12 hours during the dark cycle and catheterized after being anesthetized on isoflurane. The left common carotid artery and the right jugular vein were catheterized for sampling using a catheter with an outer diameter of 2.5 mm. The free catheter end from carotid artery was used to collect 100µl blood per 10min. The free catheter end from the jugular vein was used to infuse insulin and glucose. The insulin clamp began at 0 min with a primed-continuous infusion of human insulin

300mU/kg bolus followed by 4mU/kg/min. Normoglycemia (90–110mg/dl) is maintained during clamps by measuring blood glucose every 10min starting at *t*- 0min and infusing 10% dextrose as and when necessary. Blood samples were taken every 10min from *t*-0min to 120min and processed to determine insulin sensitivity (Figure 3C,D).

Cardiovascular measurements:

The EKG and blood pressure data was acquired using Powerlab® and LabChart® softwares from ADI instruments. A transducer was inserted in the carotid artery of the rat for recording the systolic and diastolic blood pressure. Data obtained under isoflurane anesthesia were analyzed using the LabChart® software (Figure S3b-f).

Streptozotocin (STZ) survival curve:

STZ, a pancreatic β-cell toxin, was reconstituted in chilled citrate buffer (pH = 4.5) just prior to the i.p injection. A 200 mg/Kg b.w. or lower doses of STZ were injected in fed animals *(N≥10*each). It was observed that following injection of 200mg/Kg STZ, Undernourished (but not Control) rats showed hypoglycemic convulsions and died within hours of injection. Therefore lower doses (180 mg/Kg, 125 mg/Kg, 100 mg/Kg, 60 mg/Kg and 25 mg/Kg) are used. Post-STZ survival was measured as number of rats that survived the dose on completion of day 4 since STZ injection. The high dose (200mg/Kg) of STZ rendered at least 90% Control rats diabetic, none died. However, this dose had to be reduced by eight-times in Undernourished or Recuperation rats to achieve the same effect (>90% rats diabetic and none dead post-injection). The eight-fold decrease in STZ-dose is therefore presented as increased susceptibility (Figure S3a) to STZ-induced diabetes (Figure 3E-G). Glucose was tested by Glukotest strips (Boehringer Mannheim India Ltd., Thane, India). All of the Undernourished / Recuperation rats became diabetic at the doses tested.

Immunostaining and confocal microscopy:

Anti-insulin antibody (Linco Research Inc, MO) and anti-glucagon (Sigma, St. Louis, MO) antibodies were used at 1:100 and 1:500 dilutions respectivelly. Alexa-Fluor 488, Alexa-Fluor 546 and Alexa-Fluor 633 F(ab')$_2$ secondary antibodies (Molecular Probes, OR) were used at 1:200 dilution. Hoechst 33342 was used to visualize nuclei. Briefly, tissues were fixed in 4% freshly prepared paraformaldehyde and then processed to obtain paraffin

sections. Following removal of paraffin and hydration of sections, tissue sections were permeabilized with chilled 50% methanol, blocked with 4% normal donkey serum and then incubated with mixture of primary antisera. Primary antibodies were incubated overnight at 4°C, washed with PBS and then incubated with the secondary antibodies at 37°C for 1 hour. All slides were washed extensively in PBS and mounted in Vectashield mountant. Confocal images were captured with Zeiss LSM Meta laser scanning microscope using a 63X/1.3 oil objective with optical slices ~0.8 µm. Magnification, laser and detector gains were set below saturation and were identical for scanning of all samples.   Results presented are representative fields confirmed from at least three different age/gender matched rat pancreas in each group (Figure S2c).

Real-time PCR:

Tissue samples were snap frozen upon removal and stored at -80°C until further processing. All samples were thawed on ice and homogenized using conventional battery operated handheld homogenizer (Sigma, St. Louis, MO). Tissue lysates were solubilized in 1 ml of Tri reagent (Sigma, St. Louis, MO) and re-suspended to ensure that all tissue lysates are solubilized. Total RNA isolated using manufacturer's instructions was quantified on ND-1000 spectrophotometer (NanoDrop Technologies, Wilmington, DE) and reverse transcribed to obtain cDNA using 'High Capacity cDNA Reverse Transcription Kit' (Applied Biosystems, Foster City, CA). Ten nanograms equivalent of cDNA was taken for gene transcript analysis using validated Assay-on-demand TaqMan PCR probe-primers (Life Technologies, Carlsbad, CA). Fold-changes were calculated after normalization for 18S rRNA using 2-ΔΔ Ct method as described earlier (Joglekar et al., 2010). Gene transcript analysis was carried out using 7500 FAST or ViiA-7 PCR systems (Life Technologies, Carlsbad, CA).

Primers used for real-time PCR were:

	Gene name	Symbol	F/ R	Sequence or Catalogue number
1	Insulin-1	*ins1*	-	Life Tech Inventoried | Rn02121433_g1
2	Insulin-2	*ins2*	-	Life Tech Inventoried | Rn01774648_g1
3	DNA methyl transferase A1	*dnmt3a1*	-	Life Tech Inventoried | Rn01027162_g1

Chromatin Immunoprecipitaion (ChIP):

Pancreatic tissues from Control, Undernourished or Recuperation rats were taken for islet isolation using a standardized procedure in the laboratory, involving collagenase digestion of the pancreas to liberate the islets from the pancreatic tissue. Islet cell clusters obtained were used for Chromatin Immunoprecipitation (ChIP) using a slight modification of existing protocols. Briefly, tissue was trypsinized for 2-3 minutes in a water bath at 37°C, washed to remove trypsin and then cross-linked using 1% formaldehyde (Sigma, St. Louis, MO). Cells were then sonicated to generate 300bp to 500bp DNA fragments. Quality and quantity of chromatin was assessed and immunoprecipitation using antibodies for specific histone modifications (Millipore, Billerica, MA) was carried out. Precipitation cocktail included protein A/G plus beads (Pierce, Pittsburgh, PA), sonicated salmon sperm DNA (Amersham Biosciences Pittsburgh, PA) and BSA (Sigma, St. Louis, MO). Rabbit IgG (Upstate, Millipore, Billerica, MA) was used as an isotype control. Chromatin was eluted using 2% SDS, 0.1 M $NaHCO_3$ and 10 mM DTT. Cross-links were reversed by incubating the eluted chromatin in 4M NaCl for $\geq$4-hours at 65°C. This was followed by proteinase-K digestion. DNA was then extracted using phenol- chloroform- isoamyl alcohol followed by two washes of 70% ethanol and finally dissolved in nuclease-free water. Real-time PCR was carried out to measure the relative amount of insulin promoter in each of the immunoprecipitated fractions using the primers 5′-GCTGTGAACTGGTTCATCAG-3′ (forward) and 5′-CTGCAGAAAGTGCTCATTGG-3' (reverse). PCR results are presented relative to Control levels in Figure S4e or log transformed and presented as radar plots for the epigenetic signatures in Figure 4B,C and S4f,g, i-l.

Histology:

Pancreas from 12-week old Control (C; N=6), Undernourished (U; N=6) and Recuperation (R2; N=10) rats were isolated, weighed after blotting excess water and fixed in paraformaldehyde. Tissues were processed to prepare paraffin blocks, sectioned at every 25µm for 5µm and alternate sections stained with Hematoxylin and Eosin. Every third of the unstained slides (spaced 150µm apart) was taken for immunostaining using a Guinea pig anti-Insulin antibody (DAKO) and an Alexa 488 secondary antibody using protocols described earlier (Joglekar et al., 2009a; Joglekar et al., 2009b). Sections were mounted using Vectashield mountant containing Hoechst 33342 and visualized on a FLoid fluorescence system (Life Technologies). Area of insulin-positive cells was measured on the entire section

(final magnification 460X) using blue fluorescence illumination while area of the entire pancreatic tissue was imaged using standard phase (white light). These area measurements were used to calculate beta-cell fraction in the pancreas (the ratio of insulin-positive area to the total area of the pancreatic section). Absolute beta-cell mass per pancreas was calculated as the product of mean beta-cell fraction and the corresponding pancreatic weight (mg) (Garofano et al., 1998).

Western blotting:

To assess the abundance of histone methyl transferase (KMT1A) in the pancreas of 33-week-old Control, Undernourished and Recuperation rats, pancreatic lysates were prepared in RIPA buffer and isolated protein fractions were measured on Nanodrop. A 10% resolving gel was used for SDS polyacrylamide gel electrophoresis using 20 ug of total protein per lane. Electrophoresed proteins were transferred on to membrane according to the instructions provided by the manufacturer (BioRad) and transfer was confirmed using standard Ponceau S procedure. The blot was then rinsed and non-specific epitopes were blocked using standard blocking buffer for 1-hour, washed three times in wash buffer (10 minutes each) and incubated in KMT1a antibody diluted 1:100 in blocking buffer for 1 hour at room temperature. Blots were developed using HRP conjugated secondary antibody in blocking buffer, incubated for 1-hour at room temperature and then washed in generous volumes of wash buffer. Detection reagent (Luminol) was used as per manufacturer's protocol and densitometric analysis was performed using the Bio-Rad imaging system.

Statistical analysis:

Differences between groups were calculated by using one-way or two-way ANOVA and appropriate post hoc tests. SPPS, GraphPad Prism and Jandel Scientific softwares were used to assess/plot data. A sample size of six rats in each group is sufficient to identify a difference of 27% (SD 15% of mean), with 80% power at 2p=0.05 between any two groups, or to identify a difference of 45% (SD 25% of mean) as statistically significant, with 80% power at 2p=0.05 between any two groups. Results are expressed as mean $\pm$ SEM or SD. SD (Standard Deviation) scores were used to compare organ weights of Undernourished animals in comparison to the Controls. SD score $= \sum [(x_i - X_c)/SD_c]$; wherein x_i is individual value in the experimental (Undernourished or Recuperation) group, X_c is the mean value for the Control group and SD_c is the standard deviation of the Control group. Difference between

groups was tested by one-way ANOVA and Fisher's LSD test or Student's t-test, as appropriate. Serial changes in plasma glucose and insulin concentrations were tested by paired t-test or one-way ANOVA as appropriate. Computations were performed using Graphpad® Prism software. Radar plots of the data representing ChIP studies were created by logarithmically transforming fold over detectable data, using shoelace formula.

Supplemental references

Ayala, J.E., Bracy, D.P., McGuinness, O.P., and Wasserman, D.H. (2006). Considerations in the design of hyperinsulinemic-euglycemic clamps in the conscious mouse. Diabetes *55*, 390-397.

Chintinne, M., Stange, G., Denys, B., Ling, Z., In 't Veld, P., and Pipeleers, D. (2012). Beta cell count instead of beta cell mass to assess and localize growth in beta cell population following pancreatic duct ligation in mice. PloS one *7*, e43959.

Garofano, A., Czernichow, P., and Breant, B. (1998). Beta-cell mass and proliferation following late fetal and early postnatal malnutrition in the rat. Diabetologia *41*, 1114-1120.

Hughes, P.C., and Tanner, J.M. (1970). A longitudinal study of the growth of the black-hooded rat: methods of measurement and rates of growth for skull, limbs, pelvis, nose-rump and tail lengths. J Anat *106*, 349-370.

Joglekar, M.V., Joglekar, V.M., Joglekar, S.V., and Hardikar, A.A. (2009a). Human fetal pancreatic insulin-producing cells proliferate in vitro. The Journal of endocrinology *201*, 27-36.

Joglekar, M.V., Patil, D., Joglekar, V.M., Rao, G.V., Reddy, D.N., Mitnala, S., Shouche, Y., and Hardikar, A.A. (2009b). The miR-30 family microRNAs confer epithelial phenotype to human pancreatic cells. Islets *1*, 137-147.

Joglekar, M.V., Wei, C., and Hardikar, A.A. (2010). Quantitative estimation of multiple miRNAs and mRNAs from a single cell. Cold Spring Harb Protoc *2010*, pdb prot5478.

Puranik, A.S., Halade, G., Kumar, S., Mogre, R., Apte, K., Vaidya, A.D., and Patwardhan, B. (2011). Cassia auriculata: Aspects of Safety Pharmacology and Drug Interaction. Evidence-based complementary and alternative medicine : eCAM *2011*, 915240.